Journal of Computational Applied Mechanics 2025, 56(2): 506-535

DOI: 10.22059/jcamech.2024.379729.1170

RESEARCH PAPER

Stability and dynamic analysis of in-plane heterogeneous orthotropic nanoplates: effect of elastic foundation and surface layer with variable thickness

Nima Noormohammadi [*], Amir Mohammad Asadi, Pouyan Mohammadi Dashtaki

Department of Civil Engineering, Isfahan University of Technology, Isfahan 84156-83111, Iran

Abstract

This paper develops a framework for buckling and free vibration analysis of in-plane heterogeneous orthotropic nanoplates, considering nonlocal elasticity, surface effects and elastic foundation, by formulating a simple boundary method whose basis functions are set to approximately satisfy the governing equilibrium equation, as in Trefftz methods. The novelty of the work is in two points: first, the surface effects based on Gurtin-Murdoch model are formulated considering variable thickness of the nanoplate; second, for the first time, simultaneous effect of surface layer, elastic foundation and in-plane heterogeneity are investigated on the behavior of orthotropic nanoplates along with nonlocal effects, considering simple, clamped, free and guided edges. The boundary conditions are imposed by collocation, which enhances the versatility of the method, while the solution has complete continuity over the entire domain. Verification with the literature reflects very good accuracy of the implemented method. In the numerical study, it was observed that the ratio of the buckling load and the free vibration frequency, with and without nonlocal and surface effects, is larger for the cases with constant thickness than those with variable thickness. Moreover, nanoplates with free or guided edges showed less variation of the ratio with respect to the nonlocal effect, than those with simple and clamped edges.

Keywords: buckling, free vibration; surface effects; elastic foundation; nonlocal

1. Introduction

The extraordinary physical and mechanical characteristics of nano-structures are increasingly drawing attentions towards experimental, theoretical and computational analysis in the field of nanotechnology [1-3]. Because of the high expenses and difficulties in the experimental tests, great attention is nowadays given to the computational mechanics in nano-scaled structures. Simulation by the molecular dynamics (MD) and the continuum mechanics are two major trends for nano-structures. Although the former is much more accurate in terms of considering realistic atomic properties of the structure, the latter is getting popular since MD simulations usually impose tremendous computational expenses [4]. Meanwhile, since the classic mechanics fails at nanoscopic scales due to ignorance of the size effects [5], some modifications has been applied to import those effects into the classical continuum theory, which could be confirmed by the MD simulation as well, namely the non-local (NL) theory [6, 7], the couple stress theory [8], the strain gradient theory [9] and the modified nonlocal theory [10, 11], among which the nonlocal theory is very popular especially due to its simplicity of application [12]. This theory assumes that the stress at any point relates to the strain at every point of the continua.

[*] Corresponding author. Tel: +98 31 3391 3805. Email address: noormohammadi@iut.ac.ir

A vast range of nanostructures have been introduced by far, including nanorods [13, 14], nanoribbons [15], nanobeams [16-18], nanoplates and nanoshells [19-21], nanotubes [22, 23], etc. Mechanical response of nanoplates could be realized by the solution of their governing partial differential equations (PDEs). To name some, we mention semi-analytical methods [24-31], finite difference method (FDM) [32], Finite Element Method (FEM) [33], iso-geometric analysis (IGA) [34, 35], differential quadrature method (DQM) [36] and boundary methods [37, 38].

Meanwhile, nanoplates may be subjected to elastic surface effects, which can impose different properties in addition to the bulk material, and be of importance especially for infinitesimally small-sized structures. To account for that, Gurtin and Murdoch proposed mathematical simulation of the surface effects and the interfacial energies as an elastic material layer with zero thickness, totally bonded to the bulk material all over the upper and lower surfaces of the nanoplate, and having stress-strain relationship as [39],

$$\sigma^s_{\alpha\beta}=\tau^s\delta_{\alpha\beta}+(\tau^s+\lambda^s)\varepsilon_{\gamma\gamma}\delta_{\alpha\beta}+2(\mu^s-\tau^s)\varepsilon_{\alpha\beta}+\tau^s u_{\alpha,\beta}\qquad \alpha,\beta=x,y \tag{1}$$

in which λ^s,μ^s are the Lamé constants for the surface material, τ^s is the uniform surface residual stress, $\delta_{\alpha\beta}$ is the Kronecker delta, u_α is the displacement component at surface level, and $\varepsilon_{\alpha\beta}=(u_{\alpha,\beta}+u_{\beta,\alpha})/2$ is the local strain. The superscript s stands for surface parameters. For simplicity, we take the notation $\chi_{,\alpha}=\partial\chi/\partial\alpha$ throughout the text. Many studies showed considerable effect of the surface layer on static, dynamic and stability of the nanoplate, with and without nonlocal considerations. To mention some, Ansari and Sahmani considered surface stress effects on free vibration of nanoplates [40]. Assadi considered size dependent forced vibration of nanoplates with surface effects [41]. Mohammadimehr et al. investigated surface effects on buckling of microplates based on couple stress theory [42]. Karimi et al. discovered positive and negative surface effects on the buckling and free vibration response of nanoplates [43]. Kamali and Shahabian proposed analytical solutions for buckling and post-buckling of nanoplates with consideration of surface effects [44].

Besides, nanoplates could be embedded in elastic medium. The most widely used model in this regard is the Winkler-Pasternak foundation, which has emerged in many researches so far. To name some, Liew et al. investigated vibration of multilayered graphene sheets embedded in elastic medium [45]. Pradhan and Kumar analyzed free vibration of nanoplates resting on elastic foundation [46]. The combined effect of elastic foundation and surface layer was investigated by Assadi and Farshi [47]. Tong et al. studied buckling of nanoplates based on general third-order shear deformation theory with size and surface effects [48]. Mohammadimehr et al. investigated the effect of surface stress on bending and free vibration of single layered graphene sheets in elastic medium [49]. Radić et al. analyzed buckling of double orthotropic nanoplates embedded in elastic foundation [50]. Bahn-Thien et al. analyzed buckling of non-uniform nanoplates resting on elastic foundation using FEM [51].

Methods using basis functions, such as Trefftz method [52, 53], method of fundamental solutions (MFS) [54], exponential basis functions (EBF) [55, 56] and equilibrated basis functions (EqBFs) [57-59] are simple and highly accurate techniques, whose solution bases are set to almost accurately satisfy the governing PDE, so that only the boundary conditions need to be applied in order to find the deformation response. This albeit limits the extent of their application to problems defined in homogeneous media, except for EqBFs, which has been designed to satisfy the PDE regardless of the heterogeneity of the medium. Heterogeneity for nanoplates may come from sources like variable thickness, varying material properties or elastic foundation [60, 61].

This paper investigates the effect of in-plane heterogeneity on the buckling and free vibration of nanoplates resting on elastic foundation considering surface effects. First an approximate solution series is considered, then the boundary conditions are applied to give every possible combination of the basis functions which satisfy the boundary conditions. Then the PDE based on classical plate theory is applied, by a weighted residual approach, to create the corresponding eigenvalue problems to be solved. In comparison to the energy-based mesh-dependent formulated methods such as the FEM, the proposed method has the advantage that its basis functions satisfy the governing PDE independently, resulting in accuracy increase. Besides, complete continuity of the solution function due to the use of global basis functions grants high accuracy to the deformation as well as its derivatives such as moments or shear forces. On the other side, a dis-advantage with respect to localized methods such as FEM is the global spreading of any potential pollution error, due to irregularity, concavity or singularity of internal perforations, over the entire domain. This undesirable phenomenon could be healed by reformulating the method in localized techniques such as [58]. The interested reader may follow our oncoming works in this regard.

Numerical results, first verify the proposed formulation with the available literature, then study the effect of geometric characteristics, material properties, boundary conditions, and variable thickness, on the mechanical behavior of orthotropic nanoplates. It will be shown that variable thickness leads to reduction of the buckling load or free vibration frequency ratio compared to constant thickness, whose intensity depends on the edge types of the nanoplate. To the best knowledge of the authors, this is the first time that simultaneous existence of nonlocal effects, surface effects, elastic foundation and in-plane heterogeneity, are examined for nanoplates with various edge types.

2. Derivation of the governing equations

As mentioned earlier, classical elasticity theory, also referred as local theory of elasticity, cannot account for the size effects at infinitesimal dimensions, which is vital for realistic estimation of the mechanical behavior of micro/nano scaled structures. To this end, a number of nonlocal elasticity theories have been proposed by far. Eringen's theory is very popular on this subject, which relates the stress at every point to the strain at all of the material by means of a kernel function. Due to sophistication of implementing this theory in its original integral form, an alternative differential formulation is proposed as [43],

$$(1-\mu\nabla^2)\sigma_{\alpha\beta}^{nl}=\sigma_{\alpha\beta} \tag{2}$$

which is popular due to its simplicity and acceptable accuracy. The nonlocal parameter μ is related to some properties such as material constants, internal characteristic length (e.g. granular size, Carbon bonds) and the external characteristic length (e.g. physical dimensions). The superscript nl implies the nonlocal stress field, which indeed relates to the local (Cauchy) stress field. The concerning problem of the present paper considers a rectangular plate of dimensions $a\times b$ with in-plane variable material properties or thickness, resting on elastic foundation and subjected to surface stress effects, occasionally loaded within the plane as shown in Fig 1. By ignoring the in-plane displacements of the mid-plane, the only independent deformation component will be the out-of-plane displacement $w=w(x,y,t)$. Then the curvatures in CPT are derived as,

$$\boldsymbol{\kappa}=\begin{bmatrix}\kappa_{xx} & \kappa_{yy} & \kappa_{xy}\end{bmatrix}^{\mathrm{T}}=\begin{bmatrix}w_{,xx} & w_{,yy} & 2w_{,xy}\end{bmatrix}^{\mathrm{T}} \tag{3}$$

The in-plane normal and shear strain components are related to the curvatures as,

$$\boldsymbol{\varepsilon}=\begin{bmatrix}\varepsilon_{xx} & \varepsilon_{yy} & 2\varepsilon_{xy}\end{bmatrix}=-z\boldsymbol{\kappa} \tag{4}$$

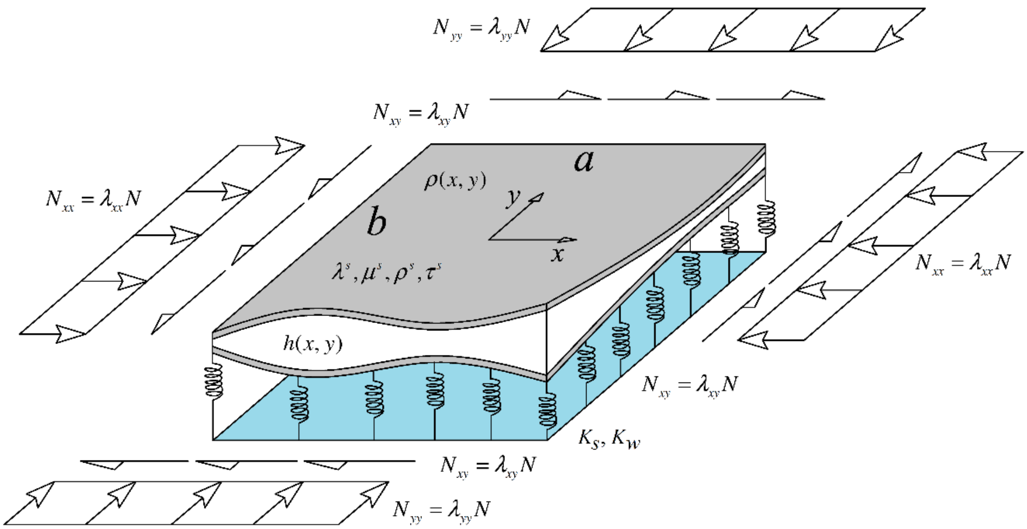

Fig 1: In-plane heterogeneous nanoplate resting on elastic foundation with surface effects.

Effect of the above mentioned components should be considered both within the bulk material of the nanoplate, and over its surface with different properties.

2.1. Effect of the bulk material

The Cauchy stress field within the bulk material may be evaluated as,

$$\sigma_{\alpha\beta}^{b}=C_{\alpha\beta\gamma\lambda}^{b}\varepsilon_{\gamma\lambda} \qquad \alpha,\beta,\gamma,\lambda\in\{x,y\} \tag{5}$$

The superscript b is indicative of the bulk material. $C_{\alpha\beta\gamma\lambda}^{b}$ is the tensor of elastic bulk material properties.

Considering the generic orthotropic material, the Cauchy stress components are evaluated as,

$$\boldsymbol{\sigma}^b = \begin{bmatrix} \sigma_{xx}^b & \sigma_{yy}^b & \sigma_{xy}^b \end{bmatrix}^T = -z\mathbf{C}^b \boldsymbol{\kappa} \tag{6}$$

z is the through thickness elevation from the mid-plane. The matrix of the bulk material constants in principal axes for plane stress condition is,

$$\mathbf{C}^b = \frac{1}{1-\nu_{xy}\nu_{yx}} \begin{bmatrix} E_x & E_x\nu_{xy} & 0 \\ E_y\nu_{yx} & E_y & 0 \\ 0 & 0 & G_{xy}\left(1-\nu_{xy}\nu_{yx}\right) \end{bmatrix} \tag{7}$$

$E_{x(y)}$ is the modulus of elasticity along $x(y)$, ν_{xy} is the Poisson's ratio and G_{xy} is the in-plane shear modulus. By integrating the above stresses through thickness, the local moments per unit length, resulted from the stress field within the bulk material, will be,

$$\mathbf{M}^b = \begin{bmatrix} M_{xx}^b & M_{yy}^b & M_{xy}^b \end{bmatrix}^{\mathrm{T}} = -\int_{-h/2}^{h/2} \begin{bmatrix} \sigma_{xx} & \sigma_{yy} & \tau_{xy} \end{bmatrix}^{\mathrm{T}} z dz = \mathbf{D}^b \boldsymbol{\kappa} \tag{8}$$

h is the (variable) thickness of the nanoplate, see Fig 1. $\mathbf{D}^b = \mathbf{C}^b h^3/12$ is the bending stiffness matrix of the bulk material [62].

2.2. Effect of the surface material

The effect of surface energy according to Gurtin-Murdoch hypothesis is imported as additional moments and shear forces through incorporation of the upper and lower surfaces of the nanoplate. So the variable thickness of the nanoplate (h) which causes an altering torque arm between the two surfaces, will enquire a reformulation of the resultants by the surface effects, since its derivatives will not vanish and thus, inserts additional terms into the equilibrium equation. According to (1), the in-plane stress components at the upper ($s+$) and lower ($s-$) surfaces of the nanoplate are derived as [41],

$$\begin{aligned} \sigma_{xx}^{s\pm} &= \tau^s \mp \frac{h}{2}\left[\left(2\mu^s + \lambda^s\right)w_{,xx} + \left(\lambda^s + \tau^s\right)w_{,yy}\right] \\ \sigma_{yy}^{s\pm} &= \tau^s \mp \frac{h}{2}\left[\left(2\mu^s + \lambda^s\right)w_{,yy} + \left(\lambda^s + \tau^s\right)w_{,xx}\right] \\ \sigma_{xy}^{s\pm} &= \mp \frac{h}{2}\left(2\mu^s - \tau^s\right)w_{,xy} \end{aligned} \tag{9}$$

The transverse shear stresses are also given as,

$$\sigma_{xz}^{s\pm} = \tau^s w_{,x}, \qquad \sigma_{yz}^{s\pm} = \tau^s w_{,y} \tag{10}$$

In addition to (9) and (10), the effect of normal surface stress along z should also be considered on in-plane stresses of the bulk material. This normal stress is derived as a result of applying the equilibrium along z at the two surfaces as,

$$\sigma_{xz,x}^s + \sigma_{yz,y}^s + \sigma_{zz,z}^s = \rho^s w_{,tt} \tag{11}$$

where ρ^s is the surface density and t is the time. Considering (10) for both upper and lower surfaces, the normal stress within the bulk material assuming linear variation will be [40],

$$\begin{aligned} \sigma_{zz}^b = &\frac{\left(\tau^s w_{,xx} + \tau^s w_{,yy} - \rho^s w_{,tt}\right)_{s+} + \left(\tau^s w_{,xx} + \tau^s w_{,yy} - \rho^s w_{,tt}\right)_{s-}}{2} \\ &+ \frac{z}{h}\left[\left(\tau^s w_{,xx} + \tau^s w_{,yy} - \rho^s w_{,tt}\right)_{s+} - \left(\tau^s w_{,xx} + \tau^s w_{,yy} - \rho^s w_{,tt}\right)_{s-}\right] \end{aligned} \tag{12}$$

Since the expression in the parentheses above is symmetric at the two surfaces, the following final relation may be suggested for the z stress within the bulk material,

$$\sigma_{zz}^{b}=\frac{2z}{h}\left(\tau^{s}w_{,xx}+\tau^{s}w_{,yy}-\rho^{s}w_{,tt}\right) \tag{13}$$

The above normal stress affects the in-plane normal stresses under the rationality that the normal strains along x and y due to this stress should become zero,

$$\begin{aligned}&\frac{\sigma_{xx}^{b,z}}{E_x}-\nu_{xy}\frac{\sigma_{yy}^{b,z}}{E_y}-\nu_{xz}\frac{\sigma_{zz}^{b}}{E_z}=0\\&-\nu_{yx}\frac{\sigma_{xx}^{b,z}}{E_x}+\frac{\sigma_{yy}^{b,z}}{E_y}-\nu_{yz}\frac{\sigma_{zz}^{b}}{E_z}=0\end{aligned} \tag{14}$$

The above relationships give,

$$\begin{aligned}\sigma_{xx}^{b,z}&=\frac{E_x\left(\nu_{xz}+\nu_{xy}\nu_{yz}\right)}{E_z\left(1-\nu_{xy}\nu_{yx}\right)}\sigma_{zz}^{b}=\eta_x\sigma_{zz}^{b}\\\sigma_{yy}^{b,z}&=\frac{E_y\left(\nu_{yz}+\nu_{yx}\nu_{xz}\right)}{E_z\left(1-\nu_{xy}\nu_{yx}\right)}\sigma_{zz}^{b}=\eta_y\sigma_{zz}^{b}\end{aligned} \tag{15}$$

For isotropic materials with elastic modulus E and Poisson's ratio ν, the above relations will simply give [40],

$$\eta_x=\eta_y=\nu/(1-\nu) \tag{16}$$

The moments by the above surface stresses may be simply written as,

$$\begin{aligned}M_{xx}^{s}&=\frac{h}{2}\left(\sigma_{xx}^{s+}-\sigma_{xx}^{s-}\right)+\int_{-h/2}^{h/2}\sigma_{xx}^{b,z}\\&=\underbrace{\left[-\frac{h^2}{2}\left(2\mu^{s}+\lambda^{s}\right)+\eta_x\frac{h^2}{6}\tau^{s}\right]}_{-D_{11}^{s}}w_{,xx}+\underbrace{\left[-\frac{h^2}{2}\left(\lambda^{s}+\tau^{s}\right)+\eta_x\frac{h^2}{6}\tau^{s}\right]}_{-D_{12}^{s}}w_{,yy}-\eta_x\frac{h^2}{6}\rho^{s}w_{,tt}\end{aligned} \tag{17}$$

$$\begin{aligned}M_{yy}^{s}&=\frac{h}{2}\left(\sigma_{yy}^{s+}-\sigma_{yy}^{s-}\right)+\int_{-h/2}^{h/2}\sigma_{yy}^{b,z}zdz\\&=\underbrace{\left[-\frac{h^2}{2}\left(\lambda^{s}+\tau^{s}\right)+\eta_y\frac{h^2}{6}\tau^{s}\right]}_{-D_{21}^{s}}w_{,xx}+\underbrace{\left[-\frac{h^2}{2}\left(2\mu^{s}+\lambda^{s}\right)+\eta_y\frac{h^2}{6}\tau^{s}\right]}_{-D_{22}^{s}}w_{,yy}-\eta_y\frac{h^2}{6}\rho^{s}w_{,tt}\end{aligned} \tag{18}$$

$$M_{xy}^{s}=\frac{h}{2}\left(\sigma_{xy}^{s+}-\sigma_{xy}^{s-}\right)=\underbrace{-\frac{h^2}{4}\left(2\mu^{s}-\tau^{s}\right)}_{-D_{33}^{s}}\left(2w_{,xy}\right) \tag{19}$$

The above relationships may be concisely written in the form below,

$$\mathbf{M}^{s}=\mathbf{D}^{s}\boldsymbol{\kappa}-\boldsymbol{\eta}w_{,tt}\qquad \boldsymbol{\eta}=\rho^{s}\frac{h^2}{6}\begin{bmatrix}\eta_x & \eta_y & 0\end{bmatrix}^{\mathrm{T}} \tag{20}$$

The nonzero components of the 3×3 matrix $\mathbf{D}^{s}$ are specified in (17)-(19).

2.3. The equilibrium and boundary conditions

The total local moments considering both the bulk and surface effects may be written as,

$$\mathbf{M}=\mathbf{M}^{b}+\mathbf{M}^{s}=\mathbf{D}\boldsymbol{\kappa}-\boldsymbol{\eta}w_{,tt}\qquad \mathbf{D}=\mathbf{D}^{b}+\mathbf{D}^{s} \tag{21}$$

Introducing (21) into (2), the nonlocal moments will be entered as,

$$(1-\mu\nabla^2)\mathbf{M}^{nl} = \mathbf{M} \tag{22}$$

The nonlocal shear forces per unit length, considering both the effect of varying moments and the transverse surface shear stresses, are then written as [40],

$$\begin{aligned} Q_x^{nl} &= M_{xx,x}^{nl} + M_{xy,y}^{nl} + \sigma_{xz}^{s+} + \sigma_{xz}^{s-} = M_{xx,x}^{nl} + M_{xy,y}^{nl} + 2\tau^s w_{,x} \\ Q_y^{nl} &= M_{yx,x}^{nl} + M_{yy,y}^{nl} + \sigma_{yz}^{s+} + \sigma_{yz}^{s-} = M_{yx,x}^{nl} + M_{yy,y}^{nl} + 2\tau^s w_{,y} \end{aligned} \tag{23}$$

Then, the equilibrium of forces for an element of unit edges along z, considering in-plane applied loads, results,

$$Q_{x,x}^{nl} + Q_{y,y}^{nl} + N_{xx}w_{,xx} + N_{yy}w_{,yy} + 2N_{xy}w_{,xy} - k_w w + k_s\nabla^2 w = m_0 w_{,tt} + m_2\nabla^2 w_{,tt} \tag{24}$$

$\nabla^2 = \partial^2/\partial x^2 + \partial^2/\partial y^2$ is the Laplacian operator. k_s and k_w are the parameters of the elastic foundation based on the Winkler-Pasternak model. $N_{\alpha\beta}$ is the applied in-plane load. m_0 and m_2 are respectively the translational and rotational moments of inertia, including both the bulk and surface effects, and defined as [43],

$$m_0 = \int_{-h/2}^{h/2} \rho^b dz + 2\rho^s \qquad m_2 = \int_{-h/2}^{h/2} \rho^b z^2 dz + \rho^s h^2 \tag{25}$$

ρ^b is the volume density of the bulk material. For homogeneous material with respect to z, the above relationships give,

$$m_0 = \rho^b h + 2\rho^s \qquad m_2 = \rho^b h^3/12 + \rho^s h^2 \tag{26}$$

By substituting (23) in (24), we will have,

$$\begin{aligned} &M_{xx,xx}^{nl} + 2M_{xy,xy}^{nl} + M_{yy,yy}^{nl} + 2\tau^s\nabla^2 w + N_x w_{,xx} + N_y w_{,yy} + 2N_{xy}w_{,xy} - k_w w + k_s\nabla^2 w \\ &= m_0 w_{,tt} + m_2\nabla^2 w_{,tt} \end{aligned} \tag{27}$$

Now, applying $1-\mu\nabla^2$ to (27), considering (21) and (22), and also the time-harmonic displacement function as $w(x,y,t) = W(x,y)\sin\omega_n t$, yields the final equilibrium equation as,

$$\begin{aligned} &-D_{11}W_{,xxxx} - 2D_{11,x}W_{,xxx} - D_{11,xx}W_{,xx} - D_{12}W_{,xxyy} - 2D_{12,x}W_{,xyy} - D_{12,xx}W_{,yy} \\ &-4D_{33}W_{,xxyy} - 4D_{33,y}W_{,xxy} - 4D_{33,x}W_{,xyy} - 4D_{33,xy}W_{,xy} - D_{21}W_{,xxyy} - 2D_{21,y}W_{,xxy} - D_{21,yy}W_{,xx} \\ &-D_{22}W_{,yyyy} - 2D_{22,y}W_{,yyy} - D_{22,yy}W_{,yy} + (2\tau^s + k_s)\nabla^2 W - k_w W \\ &+N_{xx}W_{,xx} + 2N_{xy}W_{,xy} + N_{yy}W_{,yy} + \omega_n^2\left(m_0 W + m_2\nabla^2 W\right) \\ &+\mu\Big[-2\tau^s\nabla^4 W + k_w W_{,xx} + 2k_{w,x}W_{,x} + k_{w,xx}W + k_w W_{,yy} + 2k_{w,y}W_{,y} + k_{w,yy}W - k_s\nabla^4 W \\ &\quad -2k_{s,x}\nabla^2 W_{,x} - 2k_{s,y}\nabla^2 W_{,y} - (k_{s,xx} + k_{s,yy})\nabla^2 W \\ &\quad -N_{xx}\nabla^2 W_{,xx} - 2N_{xy}\nabla^2 W_{,xy} - N_{yy}\nabla^2 W_{,yy} \\ &\quad -\omega_n^2\Big(m_0\nabla^2 W + 2m_{0,x}W_{,x} + 2m_{0,y}W_{,y} + (\nabla^2 m_0)W \\ &\qquad +m_2\nabla^4 W + 2m_{0,x}\nabla^2 W_{,x} + 2m_{0,y}\nabla^2 W_{,y} + (\nabla^2 m_0)\nabla^2 W\Big)\Big] = 0 \end{aligned} \tag{28}$$

in which $W = W(x,y)$ is the time-independent part of the lateral displacement, and ω_n is the natural frequency of free vibration. The above equation considers in-plane variation of the stiffness matrix $\mathbf{D}$, the thickness, the elastic foundation parameters and the density. This equation should be accompanied by the following boundary conditions [62],

Table 1: Various boundary conditions applied to the problem.

Edge type	Identifier	*Conditions*	
Simply supported	S	$W=0$	$M_n=0$
Clamped	C	$W=0$	$\partial W/\partial n=0$
Free	F	$V_n=0$	$M_n=0$
Guided	G	$V_n=0$	$\partial W/\partial n=0$

The components of the above table are,

$$M_n = n_x^2 M_x + n_y^2 M_y + 2n_x n_y M_{xy} \tag{29}$$

$$V_n = n_x V_x + n_y V_y \tag{30}$$

$\mathbf{n}=[n_x, n_y]^T$ is the unit normal to the boundary. Also the shear forces per unit length are,

$$V_x = \frac{\partial M_x}{\partial x} + \frac{\partial M_{xy}}{\partial y}, \quad V_y = \frac{\partial M_{xy}}{\partial x} + \frac{\partial M_y}{\partial y} \tag{31}$$

3. Development of the solution method

The time-independent part of displacement is approximated via the following double series,

$$\begin{aligned} &W(x,y) \simeq \hat{W}(\xi,\eta) = \sum_{n=0}^{O_y}\sum_{m=0}^{O_x} c_{mn} T_m(\xi) T_n(\eta) = \mathbf{f}^{\mathrm{T}}\mathbf{c} \\ &\mathbf{f} = \left[T_0(\xi)T_0(\eta) \ \ \cdots \ \ T_{O_x}(\xi)T_0(\eta) \ \ T_0(\xi)T_1(\eta) \ \ \cdots \ \ T_{O_x}(\xi)T_{O_y}(\eta) \right]^{\mathrm{T}} \\ &\mathbf{c} = \left[c_{00} \ \ \cdots \ \ c_{O_x 0} \ \ c_{01} \ \ \cdots \ \ c_{O_x O_y} \right]^{\mathrm{T}} \end{aligned} \tag{32}$$

$T_m(\xi)$ is the Chebyshev polynomial of the first kind of order m, as a function of ξ. The normalized variables $\xi = 2x/a$ and $\eta = 2y/b$ map the nanoplate surface onto the normalized interval $[-1,+1]\times[-1,+1]$, over which these polynomials are defined [63]. a and b are the edge lengths of the nanoplate, as in Fig.1. O_x and O_y are the approximation orders along x and y, respectively. The indefinite coefficients c_{mn} should be defined so that the above series satisfies the equilibrium equation in (28) and the boundary conditions in Table 1. To this end, first the boundary conditions should be applied to the approximated solution series, as a means to find any possible combination of the basis functions capable of satisfying the boundary conditions. Therefore, a proper number of boundary points are distributed over the boundaries of the nanoplate. To ensure sufficient satisfaction of the boundary conditions, the following nodal spacing should be obeyed [64],

$$\Delta\Gamma \le \min\left\{ \frac{a}{2O_x} \quad \frac{b}{2O_y} \right\} \tag{33}$$

This relation implies that at least two boundary points should exist at every half cycle of the basis function with the highest order. Assuming n_B boundary points, two conditions according to the edge type should be applied at every point, which results the following homogeneous equation at ith boundary point ($\mathbf{x}_{Bi}$),

$$\mathbf{B}\hat{W}\Big|_{\mathbf{x}=\mathbf{x}_{Bi}} = \mathbf{B}\mathbf{f}^T\Big|_{\mathbf{x}=\mathbf{x}_{Bi}} \mathbf{c} = \mathbf{0} \tag{34}$$

The 2×1 operator $\mathbf{B}=[B_1 \quad B_2]^T$ is called the boundary operator, which includes two conditions for each edge type according to Table 1. The inner operators $B_{1,2}$ take either of the following forms according to Table 1,

$$B_1=\begin{cases}1 & \text{definite lateral displacement (S or C)}\\ \partial/\partial n & \text{definite normal rotaion (C or G)}\end{cases}$$
$$B_2=\begin{cases}B_{V_n} & \text{definite edge shear force (F or G)}\\ B_{M_n} & \text{definite edge moment (S or F)}\end{cases} \tag{35}$$

The moment and shear force operators above are defined according to (29)-(31) as,

$$B_{M_n}=n_x^2\left(D_{11}\frac{\partial^2}{\partial x^2}+D_{12}\frac{\partial^2}{\partial y^2}\right)+n_y^2\left(D_{21}\frac{\partial^2}{\partial x^2}+D_{22}\frac{\partial^2}{\partial y^2}\right)+4n_xn_y\left(D_{33}\frac{\partial^2}{\partial x\partial y}\right) \tag{36}$$

$$\begin{aligned}B_{V_n}&=n_x\left[\frac{\partial}{\partial x}\left(D_{11}\frac{\partial^2}{\partial x^2}+D_{12}\frac{\partial^2}{\partial y^2}\right)+\frac{\partial}{\partial y}\left(D_{33}\frac{\partial^2}{\partial x\partial y}\right)\right]\\&+n_y\left[\frac{\partial}{\partial x}\left(D_{33}\frac{\partial^2}{\partial x\partial y}\right)+\frac{\partial}{\partial y}\left(D_{21}\frac{\partial^2}{\partial x^2}+D_{22}\frac{\partial^2}{\partial y^2}\right)\right]\end{aligned} \tag{37}$$

D_{ij} are the material properties according to (21). Repeating (34) for all boundary points makes the homogeneous matrix equation below,

$$\mathbf{Vc}=\mathbf{0} \tag{38}$$

The matrix $\mathbf{V}$ is of dimensions $2n_B\times 2n_B$, and its rows are the result of applying the boundary operators on the basis functions of the solution series. For the above to be true, $\mathbf{c}$ must be in the null-space of $\mathbf{V}$. This null-space may be defined via its bases, set as the columns of a matrix named $\boldsymbol{\varphi}$, which is derived using some standard linear algebra algorithms such as singular value decomposition (SVD). It should be noted that the rows of $\mathbf{V}$ should be normalized prior to extraction of $\boldsymbol{\varphi}$. Any possible answer for $\mathbf{c}$ may be an arbitrary linear combination of the columns of $\boldsymbol{\varphi}$, here shown by $\boldsymbol{\varphi}_r$, as,

$$\mathbf{c}=\sum_{r=1}^{\mathrm{rank}(\boldsymbol{\varphi})}d_r\boldsymbol{\varphi}_r=\boldsymbol{\varphi}\mathbf{d}\ ,\qquad \mathbf{d}=\begin{bmatrix}d_1 & \cdots & d_{\mathrm{rank}(\boldsymbol{\varphi})}\end{bmatrix}^{\mathrm{T}} \tag{39}$$

The approximated solution series may then be rewritten as,

$$\hat{W}=\mathbf{f}^T\boldsymbol{\varphi}\mathbf{d} \tag{40}$$

The above relationship includes all possible combinations of the basis functions that satisfy the boundary conditions of the nanoplate. Since the employed collocation technique enforces the boundary conditions in strong form, and not the weak form as in FEM for instance, there will not be any interactions between the boundary conditions and the PDE satisfaction. Therefore, the collocation method has no restriction with the boundary condition operator to be enforced. Meanwhile, since global basis functions are employed, some boundary inconsistencies, such as internal sharp notches, can pollute the solution function. Some remedies for this issue may be localization or enrichment of the approximated solution function. The interested reader may see our recent work on the latter topic in [59].

The unknown coefficients in $\mathbf{d}$ should be defined via imposition of the equilibrium equation, which results an eigenvalue equation from which the critical buckling loads or the free vibration frequencies can be extracted. To this end, the equilibrium PDE is decomposed into three parts as,

$$L_1(W)+N_{cr}L_2(W)+\omega_n^2L_3(W)=0 \tag{41}$$

Considering $\{N_{xx},N_{yy},N_{xy}\}=N_{cr}\{\lambda_{xx},\lambda_{yy},\lambda_{xy}\}$ with N_{cr} being the critical buckling load and $\lambda_{\alpha\beta}$ being the coefficients of the in-plane loads, the triple parts above are,

$$
\begin{aligned}
L_1(W) = & -D_{11}W_{,xxxx} - 2D_{11,x}W_{,xxx} - D_{11,xx}W_{,xx} - D_{12}W_{,xxyy} - 2D_{12,x}W_{,xyy} - D_{12,xx}W_{,yy} \\
& - 4D_{33}W_{,xxyy} - 4D_{33,y}W_{,xxy} - 4D_{33,x}W_{,xyy} - 4D_{33,xy}W_{,xy} - D_{21}W_{,xxyy} - 2D_{21,y}W_{,xxy} \\
& - D_{21,yy}W_{,xx} - D_{22}W_{,yyyy} - 2D_{22,y}W_{,yyy} - D_{22,yy}W_{,yy} + (2\tau^s + k_s)\nabla^2 W - k_w W \\
& + \mu\Big[-2\tau^s\nabla^4 W + k_w W_{,xx} + 2k_{w,x}W_{,x} + k_{w,xx}W + k_w W_{,yy} + 2k_{w,y}W_{,y} + k_{w,yy}W - k_s\nabla^4 W \\
& \quad -2k_{s,x}\nabla^2 W_{,x} - 2k_{s,y}\nabla^2 W_{,y} - (k_{s,xx} + k_{s,yy})\nabla^2 W\Big] \\
L_2(W) = & \lambda_{xx}W_{,xx} + 2\lambda_{xy}W_{,xy} + \lambda_{yy}W_{,yy} + \mu\left(-\lambda_{xx}\nabla^2 W_{,xx} - 2\lambda_{xy}\nabla^2 W_{,xy} - \lambda_{yy}\nabla^2 W_{,yy}\right) \\
L_3(W) = & m_0 W + m_2\nabla^2 W - \mu\Big(m_0\nabla^2 W + 2m_{0,x}W_{,x} + 2m_{0,y}W_{,y} + (\nabla^2 m_0)W \\
& + m_2\nabla^4 W + 2m_{0,x}\nabla^2 W_{,x} + 2m_{0,y}\nabla^2 W_{,y} + (\nabla^2 m_0)\nabla^2 W\Big)
\end{aligned}
\tag{42}
$$

To impose the PDE in (41), after substituting the approximated solution series (40), a weighted residual approach is implemented as,

$$
\int_\Omega w_i\left((L_1 + N_{cr}L_2 + \omega_n^2 L_3)\mathbf{f}^T\boldsymbol{\varphi}\mathbf{d}\right)d\Omega = 0, \qquad i = 1,\cdots,M \tag{43}
$$

Ω is the domain of the nanoplate. w_i is the selective weight function, defined in the normalized plane corresponding to some weight points as below,

$$
w_i = (1-\xi^2)(1-\eta^2)e^{-W\left[(\xi-\xi_l)^2+(\eta-\eta_k)^2\right]}, \qquad l = 1,\cdots,n_{w2} \quad k = 1,\cdots,n_{w1} \tag{44}
$$

The weight point coordinates $\{\xi_l,\eta_k\}$ in a rectangular grid are specified based on the comprehensive studies in [64] as,

$$
\begin{aligned}
\xi_l &= -1 + (2l-1)/n_{w2}, \quad l = 1,...,n_{w2} \\
\eta_k &= -1 + (2k-1)/n_{w1}, \quad k = 1,...,n_{w1}
\end{aligned}
\tag{45}
$$

where the number of rows and columns of the grid are,

$$
n_{w1} = O_y - 3, \qquad n_{w2} = O_x - 3 \tag{46}
$$

The indices in (44) are correlated as,

$$
i = (k-1)n_{w2} + l \tag{47}
$$

The weight parameter W controls sharpness of the weight function, and may be calculated with respect to the approximation order through the following proposed relation [64],

$$
W = \begin{cases} 30 & O_{\max} \le 25 \\ 30 + 160\left(\dfrac{O_{\max}-25}{10}\right)^{2.5} + 15e^{-(O_{\max}-29)^2} & O_{\max} > 25 \end{cases} \qquad O_{\max} = \max\{O_x, O_y\} \tag{48}
$$

Evaluating (43) for all weight functions gives,

$$
(\mathbf{A}_1 + N_{cr}\mathbf{A}_2 + \omega_n^2\mathbf{A}_3)\boldsymbol{\varphi}\mathbf{d} = \mathbf{0} \tag{49}
$$

where the individual matrices are,

$$
\mathbf{A}_k = \int_\Omega \mathbf{w}L_k\mathbf{f}^T d\Omega, \qquad k = 1,2,3 \qquad \mathbf{w} = \begin{bmatrix} w_1 & w_2 & \cdots & w_M \end{bmatrix}^T \tag{50}
$$

To avoid evaluation of complicated double integrals in (50), they may be reproduced by simple algebraic combination of pre-evaluated single integrals. To this end, the variable parameters including the stiffness coefficients, the mass moments of inertia and the foundation properties should be decomposed into combination of one-dimensional (1D) functions in the form of incomplete normalized monomials from the Pascal triangle,

$$D_i = \mathbf{f}_D^T \mathbf{c}_D^i, \qquad \mathbf{f}_D = \begin{bmatrix} 1 & \xi & \cdots & \xi^{m_x} & \eta & \xi\eta & \cdots & \xi^{m_x}\eta & \cdots & \cdots & \xi^{m_x}\eta^{m_y} \end{bmatrix}^T \tag{51}$$

where D_i is indicative of the targeted variable properties. The unknown vector $\mathbf{c}_D^i$ is evaluated through point fitting of the above series with the targeted parameter over the entire nanoplate surface. Then it should be rearranged as,

$$D_i = \mathbf{f}_\xi^T \mathbf{C}_D^i \mathbf{f}_\eta, \qquad \mathbf{f}_\xi = \begin{bmatrix} 1 & \xi & \cdots & \xi^{m_x} \end{bmatrix}^T, \qquad \mathbf{f}_\eta = \begin{bmatrix} 1 & \eta & \cdots & \eta^{m_y} \end{bmatrix}^T \tag{52}$$

The entries of the middle matrix above are related to those in (51) as,

$$\left(C_D^i\right)_{p,q} = \left(c_D^i\right)_{(q-1)(m_x+1)+p}, \qquad p = 1,\ldots,m_x+1, \quad q = 1,\ldots,m_y+1 \tag{53}$$

The above matrix should be defined for the stiffness components D_{ij} shown by $\mathbf{C}_D^{ij}$, the density parameters m_0 and m_2 shown by $\mathbf{C}_m^0$ and $\mathbf{C}_m^2$ respectively, the elastic foundation parameters k_w and k_s shown by $\mathbf{C}_k^s$ and $\mathbf{C}_k^w$ respectively, and the additional terms due to consideration of the normal stress along *z*, namely ρ_x and ρ_y, shown by $\mathbf{C}_\rho^x$ and $\mathbf{C}_\rho^y$ respectively. Now the required normalized single integrals may be evaluated as the entries of the 3D matrices below,

$$\begin{aligned} \left(A_{ij}\right)_{l,m,p} &= \int_{-1}^{+1} e^{-W(\xi-\xi_l)^2} \frac{\partial^i \xi^p}{\partial \xi^i} \frac{\partial^j T_m(\xi)}{\partial \xi^j} d\xi, \\ \left(B_{ij}\right)_{k,n,q} &= \int_{-1}^{+1} e^{-W(\eta-\eta_k)^2} \frac{\partial^i \eta^q}{\partial \eta^i} \frac{\partial^j T_n(\eta)}{\partial \eta^j} d\eta, \qquad ij \in \{00,01,02,03,04,11,13,20,22\} \end{aligned} \tag{54}$$

where the counters in the above relations vary as below,

$$l(k) = 1,\ldots,n_{w2}(n_{w1}), \qquad m(n) = 0,\ldots,O_x(O_y), \qquad p(q) = 0,\ldots,m_x(m_y), \tag{55}$$

The values within parentheses are for y direction, while those outside are for x direction. Now the triple parts of (50) are composed in the following auxiliary matrices. $[\mathbf{A}_{ij}]_l$ ($[\mathbf{B}_{ij}]_k$) is the 2D matrix extracted from the 3D matrix $\mathbf{A}_{ij}$ ($\mathbf{B}_{ij}$) for the first index equal to $l(k)$, meaning correspondence of the data to lth column (kth row) of the weight grid,

$$\begin{aligned} \mathbf{A}_1^h = &-([\mathbf{A}_{04}]_l + 2[\mathbf{A}_{13}]_l + [\mathbf{A}_{22}]_l)\mathbf{C}_D^{11}[\mathbf{B}_{00}]_k^T - ([\mathbf{A}_{02}]_l + 2[\mathbf{A}_{11}]_l + [\mathbf{A}_{20}]_l)\mathbf{C}_D^{12}[\mathbf{B}_{02}]_k^T \\ &-[\mathbf{A}_{02}]_l \mathbf{C}_D^{21}([\mathbf{B}_{02}]_k^T + 2[\mathbf{B}_{11}]_k^T + [\mathbf{B}_{20}]_k^T) - [\mathbf{A}_{00}]_l \mathbf{C}_D^{22}([\mathbf{B}_{04}]_k^T + 2[\mathbf{B}_{13}]_k^T + [\mathbf{B}_{22}]_k^T) \\ &-4([\mathbf{A}_{02}]_l + [\mathbf{A}_{11}]_l)\mathbf{C}_D^{33}([\mathbf{B}_{02}]_k^T + [\mathbf{B}_{11}]_k^T) \\ &-[\mathbf{A}_{00}]_l \mathbf{C}_k^w [\mathbf{B}_{00}]_k^T + [\mathbf{A}_{02}]_l \mathbf{C}_k^s [\mathbf{B}_{00}]_k^T + [\mathbf{A}_{00}]_l \mathbf{C}_k^s [\mathbf{B}_{02}]_k^T \\ &+2\tau^s([\mathbf{A}_{02}]_l \mathbf{C}_0 [\mathbf{B}_{00}]_k^T + [\mathbf{A}_{00}]_l \mathbf{C}_0 [\mathbf{B}_{02}]_k^T) \\ &+\mu\Big[[\mathbf{A}_{02}]_l \mathbf{C}_k^w [\mathbf{B}_{00}]_k^T + [\mathbf{A}_{00}]_l \mathbf{C}_k^w [\mathbf{B}_{02}]_k^T \\ &\quad -[\mathbf{A}_{04}]_l \mathbf{C}_k^s [\mathbf{B}_{00}]_k^T - [\mathbf{A}_{00}]_l \mathbf{C}_k^s [\mathbf{B}_{04}]_k^T - 2[\mathbf{A}_{02}]_l \mathbf{C}_k^s [\mathbf{B}_{02}]_k^T \\ &\quad -2\tau^s([\mathbf{A}_{04}]_l \mathbf{C}_0 [\mathbf{B}_{00}]_k^T - [\mathbf{A}_{02}]_l \mathbf{C}_0 [\mathbf{B}_{02}]_k^T - [\mathbf{A}_{00}]_l \mathbf{C}_0 [\mathbf{B}_{04}]_k^T)\Big] \end{aligned} \tag{56}$$

$$\begin{aligned} \mathbf{A}_2^h = &\lambda_{xx}[\mathbf{A}_{02}]_l \mathbf{C}_0 [\mathbf{B}_{00}]_k^T + \lambda_{yy}[\mathbf{A}_{00}]_l \mathbf{C}_0 [\mathbf{B}_{02}]_k^T + 2\lambda_{xy}[\mathbf{A}_{01}]_l \mathbf{C}_0 [\mathbf{B}_{01}]_k^T \\ &-\mu\Big[\lambda_{xx}[\mathbf{A}_{04}]_l \mathbf{C}_0 [\mathbf{B}_{00}]_k^T + \lambda_{yy}[\mathbf{A}_{02}]_l \mathbf{C}_0 [\mathbf{B}_{02}]_k^T + 2\lambda_{xy}[\mathbf{A}_{03}]_l \mathbf{C}_0 [\mathbf{B}_{01}]_k^T \\ &\quad +\lambda_{xx}[\mathbf{A}_{02}]_l \mathbf{C}_0 [\mathbf{B}_{02}]_k^T + \lambda_{yy}[\mathbf{A}_{00}]_l \mathbf{C}_0 [\mathbf{B}_{04}]_k^T + 2\lambda_{xy}[\mathbf{A}_{01}]_l \mathbf{C}_0 [\mathbf{B}_{03}]_k^T\Big] \end{aligned} \tag{57}$$

$$\begin{aligned}
\mathbf{A}_3^h = & -[\mathbf{A}_{00}]_l \mathbf{C}_m^0 [\mathbf{B}_{00}]_k^T + [\mathbf{A}_{02}]_l \mathbf{C}_m^2 [\mathbf{B}_{00}]_k^T + [\mathbf{A}_{00}]_l \mathbf{C}_m^2 [\mathbf{B}_{02}]_k^T \\
& -([\mathbf{A}_{02}]_l + 2[\mathbf{A}_{11}]_l + [\mathbf{A}_{20}]_l)\mathbf{C}_\rho^x [\mathbf{B}_{00}]_k^T - [\mathbf{A}_{00}]_l \mathbf{C}_\rho^y ([\mathbf{B}_{02}]_k^T + 2[\mathbf{B}_{11}]_k^T + [\mathbf{B}_{20}]_k^T) \\
& + \mu \Big[([\mathbf{A}_{20}]_l + 2[\mathbf{A}_{11}]_l + [\mathbf{A}_{02}]_l)\mathbf{C}_m^0 [\mathbf{B}_{00}]_k^T + [\mathbf{A}_{00}]_l \mathbf{C}_m^0 ([\mathbf{B}_{20}]_k^T + 2[\mathbf{B}_{11}]_k^T + [\mathbf{B}_{02}]_k^T) \\
& \quad - [\mathbf{A}_{22}]_l \mathbf{C}_m^2 [\mathbf{B}_{00}]_k^T - [\mathbf{A}_{20}]_l \mathbf{C}_m^2 [\mathbf{B}_{02}]_k^T - 2[\mathbf{A}_{13}]_l \mathbf{C}_m^2 [\mathbf{B}_{00}]_k^T - 2[\mathbf{A}_{11}]_l \mathbf{C}_m^2 [\mathbf{B}_{02}]_k^T \\
& \quad - [\mathbf{A}_{04}]_l \mathbf{C}_m^2 [\mathbf{B}_{00}]_k^T - [\mathbf{A}_{02}]_l \mathbf{C}_m^2 [\mathbf{B}_{02}]_k^T - [\mathbf{A}_{02}]_l \mathbf{C}_m^2 [\mathbf{B}_{20}]_k^T - [\mathbf{A}_{00}]_l \mathbf{C}_m^2 [\mathbf{B}_{22}]_k^T \\
& \quad - 2[\mathbf{A}_{02}]_l \mathbf{C}_m^2 [\mathbf{B}_{11}]_k^T - 2[\mathbf{A}_{00}]_l \mathbf{C}_m^2 [\mathbf{B}_{13}]_k^T - [\mathbf{A}_{02}]_l \mathbf{C}_m^2 [\mathbf{B}_{02}]_k^T - [\mathbf{A}_{00}]_l \mathbf{C}_m^2 [\mathbf{B}_{04}]_k^T \\
& \quad + ([\mathbf{A}_{04}]_l + 4[\mathbf{A}_{13}]_l + 6[\mathbf{A}_{22}]_l)\mathbf{C}_\rho^x [\mathbf{B}_{00}]_k^T + [\mathbf{A}_{00}]_l \mathbf{C}_\rho^y ([\mathbf{B}_{04}]_k^T + 4[\mathbf{B}_{13}]_k^T + 6[\mathbf{B}_{22}]_k^T) \\
& \quad + ([\mathbf{A}_{02}]_l + 2[\mathbf{A}_{11}]_l + [\mathbf{A}_{20}]_l)\mathbf{C}_\rho^x [\mathbf{B}_{02}]_k^T + [\mathbf{A}_{02}]_l \mathbf{C}_\rho^y ([\mathbf{B}_{02}]_k^T + 2[\mathbf{B}_{11}]_k^T + [\mathbf{B}_{20}]_k^T) \\
& \quad + ([\mathbf{A}_{02}]_l + 2[\mathbf{A}_{11}]_l + [\mathbf{A}_{20}]_l)\mathbf{C}_\rho^x [\mathbf{B}_{20}]_k^T + [\mathbf{A}_{20}]_l \mathbf{C}_\rho^y ([\mathbf{B}_{02}]_k^T + 2[\mathbf{B}_{11}]_k^T + [\mathbf{B}_{20}]_k^T) \\
& \quad + 2([\mathbf{A}_{02}]_l + 2[\mathbf{A}_{11}]_l + [\mathbf{A}_{20}]_l)\mathbf{C}_\rho^x [\mathbf{B}_{11}]_k^T + 2[\mathbf{A}_{11}]_l \mathbf{C}_\rho^y ([\mathbf{B}_{02}]_k^T + 2[\mathbf{B}_{11}]_k^T + [\mathbf{B}_{20}]_k^T) \Big]
\end{aligned} \tag{58}$$

$\mathbf{C}_0$ is the diagonal matrix below,

$$\mathbf{C}_0 = \mathrm{Diag}\big[1, 0, 0, \ldots, 0\big] \tag{59}$$

Successive rows of $\mathbf{A}_i^h$ should be arranged next to each other to form one row of $\mathbf{A}_i$ in (49) corresponding to the weight point situated on kth row and lth column of the weight grid. Repeated for every weight point, the mentioned matrices are completed. Now the eigenvalue problems related to the buckling or free vibration may be constituted as below,

$$(\mathbf{A}_1 \boldsymbol{\varphi} + N_{cr} \mathbf{A}_2 \boldsymbol{\varphi})\mathbf{d} = \mathbf{0} \qquad \text{Buckling problem}$$

$$(\mathbf{A}_1 \boldsymbol{\varphi} + \omega_n^2 \mathbf{A}_3 \boldsymbol{\varphi})\mathbf{d} = \mathbf{0} \qquad \text{Free vibration problem} \tag{60}$$

Solution of the above problems will give,

$$N_{cr} \in \mathrm{Eigenvalues}\Big[(\mathbf{A}_2 \boldsymbol{\varphi})^+ \mathbf{A}_1 \boldsymbol{\varphi}\Big], \quad \omega_n^2 \in \mathrm{Eigenvalues}\Big[(\mathbf{A}_3 \boldsymbol{\varphi})^+ \mathbf{A}_1 \boldsymbol{\varphi}\Big] \tag{61}$$

The sign + above stands for the Moore-Penrose pseudo inversion. The unknown coefficients d form the eigenvectors in (60) for the mode shapes. One may also consider the interaction of the in-plane loads with the free vibration frequency through simultaneous consideration of the three terms above as,

$$(\mathbf{A}_1 \boldsymbol{\varphi} + N \mathbf{A}_2 + \omega_n^2 \mathbf{A}_3 \boldsymbol{\varphi})\mathbf{d} = \mathbf{0} \tag{62}$$

where N is the applied in-plane load, less than the critical buckling load of the nanoplate, which affects the stiffness of the nanoplate and thus, alters the free vibration frequencies as,

$$\omega_n^2 \in \mathrm{Eigenvalues}\Big[(\mathbf{A}_3 \boldsymbol{\varphi})^+ (\mathbf{A}_1 \boldsymbol{\varphi} + N \mathbf{A}_2 \boldsymbol{\varphi})\Big] \tag{63}$$

4. Verification

This section brings up several problems of buckling and free vibration of nanoplates from the well reputed literature, in order to verify the accuracy of the proposed formulation. The edge type sequences are addressed as in Fig 2. For instance, the edge configuration SCSF indicates simple edges 1 and 3, clamped edge 2 and free edge 4.

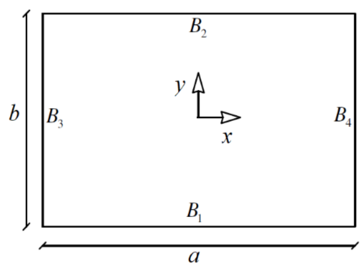

Fig 2: Rectangular nanoplate and the order of edges.

Reports include the non-dimensional critical buckling load, and the fundamental free vibration frequency as,

$$\Lambda = \omega_n a^2 \sqrt{\frac{\rho_0 t_0}{D_0}}, \quad k = \frac{N_{cr} a^2}{\pi^2 D_0}, \qquad D_0 = \frac{E_{x0} t_0^3}{12(1-\nu_{xy}\nu_{yx})} \tag{64}$$

The parameters with zero subscripts refer to a specific situation, usually the left edge of the nanoplate, unless otherwise stated. The elastic foundation parameters are imported in the normalized forms below,

$$K_S = \frac{k_s a^2}{D_0}, \qquad K_W = \frac{k_w a^4}{D_0} \tag{65}$$

The orthotropic bulk material properties are considered as [65],

$$E_x = 1765\text{GPa} \quad E_y = 1588\text{GPa} \quad \nu_{xy} = 0.3 \quad G_{xy} = 678.85\text{GPa} \tag{66}$$

Moreover, the surface properties used in case are read from [43],

$$E_s = \lambda_s + \mu_s = 5.43\,\text{N/m} \quad \tau_s = 0.9108\,\text{N/m} \quad \rho_s = 5.46\times10^{-7}\,\text{kg/m}^2 \tag{67}$$

In all examples of this section, the effect of normal stress σ_{zz} is ignored, in accordance with the selected references. For the solution method, the effective parameters are set unchangingly as below, and the rest of the parameters are defined based on then,

$$O_x = O_y = 20, \qquad m_x = m_y = 3, \qquad n_B = 160 \tag{68}$$

4.1. Buckling examples

The first example examines a simply supported square nanoplate with edge length $a = b = 15\text{nm}$ and constant thickness $h = 0.34\text{nm}$, resting on elastic foundation with $K_S = 0$ and variable K_W, for various nonlocal values. The material is isotropic with $E = 1.06\text{TPa}$ and $\nu = 0.25$. Fig 3 compares the results for the following buckling load ratio by the present method with those in [51], in which excellent confirmation was achieved,

$$\lambda = \frac{\text{Buckling load with nonlocal effect}}{\text{Buckling load without nonlocal effect}} \tag{69}$$

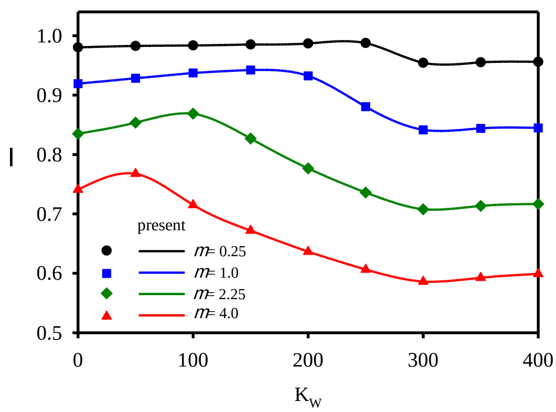

Fig 3. Buckling load ratio (69) of SSSS square nanoplate versus K_W for various nonlocal parameters - lines: present method, markers: [51] ($K_S = 0$, $a = 15\text{nm}$, $h = 0.34\text{nm}$, $\lambda_{xx} = \lambda_{yy} = 1$)

The next example considers a square nanoplate with edge length $a = b = 10\text{nm}$, constant thickness $h = 2\text{nm}$ with surface effects but without elastic foundation. The bulk material is isotropic with $E = 70\text{GPa}$ and $\nu = 0.3$, while the surface properties are as in (67). The reported buckling load ratio as below,

$$\lambda = \frac{\text{Buckling load with nonlocal and surface effects}}{\text{Buckling load with nonlocal but without surface effects}} \tag{70}$$

which is compared with [43] in Fig 4, reveals perfect application of the proposed formulation. Notable is that the nonlocal length in Fig 4 relates to the nonlocal parameter through $\mu = g^2$. This example confirms applicability of the proposed formulation in case of the existence of surface effects with various boundary conditions.

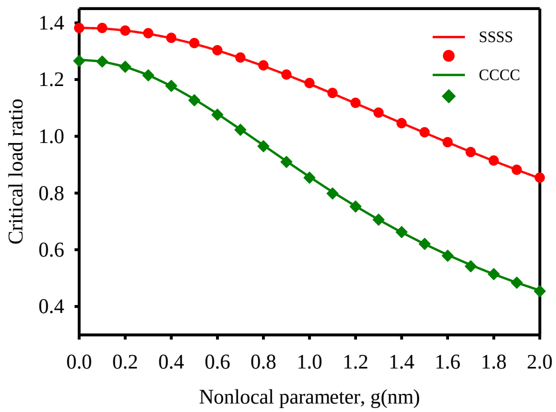

Fig 4. Buckling load ratio (70) of square nanoplate versus nonlocal parameter $g = \sqrt{\mu}$ without elastic foundation - lines: present, markers: [43] ($a = 10\text{nm}$, $h = 2\text{nm}$, $\lambda_{xx} = \lambda_{yy} = 1$)

The final example of this section considers biaxial buckling of SSSS square nanoplate of edge 10nm and minimum thickness $h_0 = 0.34\text{nm}$, with linearly variable thickness as,

$$h = h_0\left(1+\gamma\left(\frac{x+a/2}{a}\right)\right) \tag{71}$$

The orthotropic material properties are as in (66). Results presented in Fig 5 without surface effects or elastic foundation, compared with [60], reveal perfect confirmation of the present formulation, and its application for problems with variable thickness.

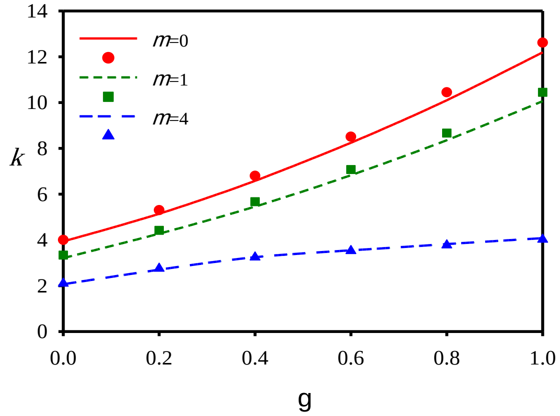

Fig 5. Non-dimensional buckling load of SSSS square nanoplate with linear thickness for various nonlocal parameters without surface effects or elastic foundation - markers: present, lines: [60] ($a = 15\text{nm}$, $\lambda_{xx} = \lambda_{yy} = 1$)

4.2. Free vibration examples

In this section, a number of sample problems are revisited to examine the applicability and performance of the method in free vibration problems. First, to show the effect of elastic foundation on free vibration frequencies, a square plate of side length 10m and thickness 15cm is considered, without any non-local effects. The material properties are $E = 25\text{GPa}$, $\nu = 0.15$ and $\rho = 2250\,\text{kg/m}^3$. For fully clamped or simply supported edges, the normalized free vibration frequencies Λ_{ij}, with i and j being the number of half-waves along each direction, are compared with those reported in [66], for various values of Winkler-Pasternak foundation parameters. Results are normalized as in (64). The agreement of results is an evidence for proper performance of the proposed method in this case.

Table 2. Non-dimensional free vibration frequencies of square plate without non-local effects resting on elastic foundation.

	k_w (kN/m^3)	k_s (MPa)	Λ_{11}		Λ_{21}	
			Present	[66]	Present	[66]
CCCC	100000	0	51.807	51.902	82.278	83.222
	200000	0	63.824	63.759	90.324	91.276
	100000	120	80.689	80.314	126.793	127.294
SSSS	100000	0	42.181	42.282	61.822	62.417
	200000	0	56.293	56.376	72.186	72.707
	100000	120	71.211	71.365	109.758	110.963

Next, to see the performance with non-local effects, a square plate of side length 10nm and thickness 0.34nm, having material properties $E = 1.06\text{TPa}$, $\nu = 0.25$ and $\rho = 2250\,\text{kg/m}^3$, is considered resting on Winkler-Pasternak elastic foundation. Table 3 compares the results for the following frequency ratio by the present method, with those presented in [67],

$$\varpi = \frac{\text{Frequency with nonlocal effect}}{\text{Frequency without nonlocal effect}} \tag{72}$$

It should be noted that the mentioned reference has considered visco-elastic foundation properties, which has affected its results. However, proper confirmation is visible between the results from the two sources, which shows applicability of the method in this case as well.

Table 3. Frequency ratios as (72) of square nanoplate with non-local effects resting on elastic foundation.

μ	K_W	K_S	ϖ_{11}		ϖ_{21}	
			Present	[67]	Present	[67]
0	50	10	0.5346	0.5419	0.8850	0.8971
	100	20	0.7299	0.7399	1.1507	1.1665
	200	30	0.9108	0.9233	1.3838	1.4027
1	50	10	0.5286	0.5358	0.8386	0.8500
	100	20	0.7255	0.7354	1.1154	1.1307
	200	30	0.9073	0.9197	1.3545	1.3731
2	50	10	0.5242	0.5314	0.8142	0.8253
	100	20	0.7223	0.7322	1.0972	1.1122
	200	30	0.9047	0.9171	1.3396	1.3579
3	50	10	0.5209	0.5280	0.7991	0.8101
	100	20	0.7199	0.7298	1.0861	1.1009
	200	30	0.9028	0.9152	1.3305	1.3487

Next, performance of the method is examined for existence of surface effects. This example also shows the ability of the method to accurately extract the free vibration frequencies in the presence of in-plane normal or shear loads N_x, N_y, N_{xy}, which are imported in normalized form as $k = N_{\alpha\beta}a^2/D$, for various values of the nonlocal parameter μ or the in-plane load, in Tables 4 and 5. The selected square nanoplate has edge length 10nm and thickness 2nm. The reported values are the ratio of the principal frequency value while considering the nonlocal and the surface effects, to the case with nonlocal but without surface effects. As seen, the results are in excellent agreement with those by analytical approach from [43].

Table 4. Frequency ratios of square nanoplate with surface effects, in-plane loads and various non-local parameters.

In-plane load type	Edges	$\mu=0$		$\mu=1$		$\mu=1.44$	
		Present	[43]	Present	[43]	Present	[43]
Biaxial ($k=10$)	CCCC	1.146	1.147	1.189	1.190	1.210	1.210
	SCSC	1.198	1.200	1.259	1.260	1.288	1.288
	SSSS	1.327	1.330	1.4291	1.430	1.494	1.495
Shear ($k=10$)	CCCC	1.124	1.125	1.1439	1.145	1.153	1.154
	SCSC	1.146	1.147	1.165	1.166	1.173	1.174
	SSSS	1.176	1.178	1.196	1.197	1.199	1.206

Table 5. Frequency ratios of square nanoplate with surface effects and variable in-plane load ($\mu = 1\text{nm}^2$).

In-plane load type	Edges	Dimensionless in-plane load value (k)					
		0		6		14	
		Present	[43]	Present	[43]	Present	[43]
Biaxial	CCCC	1.142	1.143	1.168	1.169	1.232	1.233
	SSCC	1.162	1.163	1.200	1.209	1.350	1.351
	SSSS	1.193	1.194	1.285	1.286	1.943	1.944
Shear	CCCC	1.141	1.142	1.142	1.143	1.147	1.148
	SSCC	1.161	1.162	1.162	1.163	1.170	1.171
	SSSS	1.190	1.191	1.193	1.194	1.199	1.203

To extend the range of validation, a square nanoplate of edge 50nm with various thickness values is selected. The nonlocal parameter is fixed at $\mu = 1\text{nm}^2$, and the biaxial or shear in-plane load is also adjusted as $k = 10$. Table 6 shows great performance of the present method for various thickness values.

Table 6. Frequency ratios of square plate with surface effects and variable thickness ($\mu = 1\text{nm}^2$, $k = 10$).

In-plane load type	Edges	Plate thickness (nm)					
		1		1.5		2	
		Present	[43]	Present	[43]	Present	[43]
Biaxial	CCCC	4.098	4.103	2.450	2.454	1.775	1.776
	SSCC	5.639	5.645	3.258	3.259	3.279	2.280
	SSSS	8.743	8.748	4.858	4.859	3.268	3.269
Shear	CCCC	3.706	3.711	2.230	2.231	1.682	1.683
	SSCC	4.365	4.371	2.748	2.750	1.979	1.981
	SSSS	6.159	6.163	3.479	3.481	2.393	2.394

Although the previous results confirm the method for clamped and simple boundary conditions, the results in Table 7 are also brought to show its performance with free edges. The considered nanoplate is a square of edge 10nm and thickness 0.34nm, with the orthotropic material properties as in (66), and $\rho = 2300\,\text{kg}/\text{m}^3$. As seen, perfect agreement is achieved with the analytical results from [68], which is a firm evidence of methods' applicability for nanoplates with free edges.

Table 7. Non-dimensional higher mode frequencies of square nanoplate.

Edges type	μ	Source	Mode number			
			1	2	3	4
SSFF	0	Present	9.16	15.88	36.57	37.00
		Xu et al. [68]	9.16	15.88	36.57	37.00
	1	Present	8.80	15.16	31.69	32.85
		Xu et al. [68]	8.80	15.16	31.69	32.85
	2	Present	7.92	13.45	23.58	26.12
		Xu et al. [68]	7.92	13.45	23.58	26.12
	4	Present	5.96	9.86	14.12	16.64
		Xu et al. [68]	5.96	9.86	14.12	16.64
SSCF	0	Present	12.34	32.86	39.87	61.62
		Xu et al. [68]	12.34	32.86	39.87	61.62
	1	Present	11.82	29.61	33.98	49.77
		Xu et al. [68]	11.82	29.61	33.98	49.77
	2	Present	10.57	23.62	21.13	34.78
		Xu et al. [68]	10.57	23.62	21.12	34.78
	4	Present	7.87	14.96	15.00	19.91
		Xu et al. [68]	7.87	14.96	15.00	19.91

Finally, to show that the method is also applicable for free vibration analysis of plates with variable thickness, the last table of this section gives the non-dimensional frequencies of the first two modes for a square plate without nonlocal effects. The thickness varies linearly as in (71), and the material is isotropic. Results compared with the exact solutions from [69] in Table 8 reveal perfect accuracy, another sign that the proposed method is applicable for plates with variable thickness.

Table 8: Non-dimensional free vibration frequencies of square plate with linear varying thickness, without nonlocal effects.

Edges	γ	Present		Exact [69]	
		Mode 1	Mode 2	Mode 1	Mode 2
CCCC	0.2	39.52	80.53	39.51	80.52
	0.4	42.90	87.29	42.91	87.29
SSSS	0.2	21.69	54.16	21.69	54.16
	0.4	23.61	58.77	23.61	58.78
SSCC	0.2	29.72	66.11	29.73	66.12
	0.4	32.33	71.36	32.34	71.37

Now that the method has been verified, to see its convergence progress and stability, Table 9 presents the biaxial buckling load and the first four free vibration frequencies, normalized as in (64), for square simply supported and clamped nanoplates with surface effects, with respect to the effective parameter of approximation order $O_x = O_y$. The number of boundary points follows the rule in (33) for every case. As seen, the response converges to the final value very fast, and remains unchanged up to much higher orders. This is a confirmation of proper convergence and stability of the proposed method.

Table 9: Non-dimensional free vibration frequencies of square plate with linear varying thickness, without nonlocal effects.

	Edge types	Mode number	$O_x = O_y$				
			5	7	10	15	20
Free vibration	SSSS	1	20.7350	19.3853	19.3973	19.3973	19.3973
		2, 3	36.0703	37.1612	37.4749	37.4676	37.4676
		4	48.1574	49.5505	49.8900	49.8825	49.8825
	CCCC	1	37.1508	32.1091	32.3129	32.3143	32.3143
		2, 3	50.4834	49.3851	50.9480	50.9325	50.9325
		4	62.1540	60.7045	62.2271	62.2259	62.2259
Buckling	SSSS	1	2.1359	2.0568	2.0585	2.0585	2.0585
	CCCC	1	4.3322	3.4224	3.4530	3.4530	3.4530

After validation, the next section will present the numerical results gained by the proposed method for various cases of interest.

5. Results and discussion

This section presents several simulations of buckling and free vibration of nanoplates with various properties regarding nonlocal and geometric parameters, surface effects or elastic foundation. Numerous parameters are effective in the structural response of the nanplate, including geometric parameters, nonlocal effects, surface effects and elastic foundation. The thickness may be variable according to,

$$h = h_0\left(1+\gamma\left(\frac{x+a/2}{a}\right)^n\right) \tag{73}$$

h_0 is the thickness at the left edge of the nanoplate. n is equal to 0, 1 or 2 for constant, linear or quadratic thickness variation. γ defines the thickness difference of the left and right edges for the cases with variable thickness; for instance $\gamma = 1$ gives the right edge thickness twice that at the left edge. The following diagrams depict effect of various parameters on the buckling load or fundamental frequency of the nanoplate. Whenever not stated otherwise, the following parameters have been considered,

$$a = 15\text{nm},\quad b/a = 1,\quad h = 1\text{nm},\quad \mu = 1\text{nm}^2,\quad K_W = 200,\quad K_S = 0 \tag{74}$$

The orthotropic bulk material properties are the same as (66). Also, the surface effects are considered as [41]:

$$\lambda_s = 5.263\,\text{N/m},\quad \mu_s = 2.256\,\text{N/m},\quad \tau_s = 0.9108\,\text{N/m},\quad \rho_s = 5.46\times10^{-7}\,\text{kg/m}^2 \tag{75}$$

Selection of the nonlocal elasticity parameters in (66) and (75) for nanoplate of variable thickness may be rationalize from the probability that multiple graphene sheets of unequal area could be laid over each other in a layered structure. Ignoring the van der Waals effects among the successive layers, leads to an equivalent single-layered nanoplate with variable thickness. Now, the effect of surface energy may be applied as in a single layered graphene sheet, but with consideration of variable thickness, which alters the torque arm between the upper and lower surfaces over the surface of the nanoplate. The principal method properties for the solution of the related problems are the following values, and the others will be defined correspondingly,

$$O_x = O_y = 20, \quad m_x = m_y = 6, \quad N_B = 160 \tag{76}$$

5.1. Buckling analysis

This subsection gives the results for buckling of nanoplates under various circumstances. To give a comprehensive insight, the following buckling load ratio will be reported for comparison of different cases,

$$\lambda = \frac{\text{Critical buckling load with size effect, surface effect or elastic foundation}}{\text{Critical buckling load without size effect, surface effect and elastic foundation}} \tag{77}$$

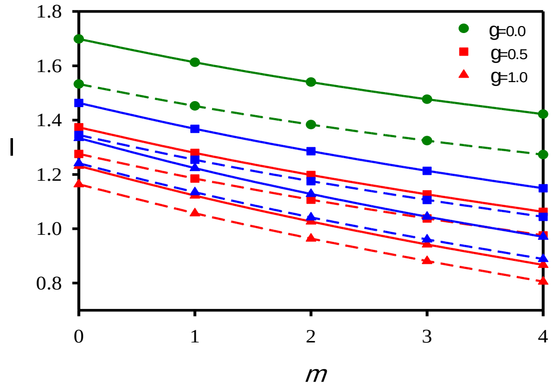

Fig 6. Biaxial buckling load ratio of SSSS square nanoplate with constant (green), linear (blue) and quadratic (red) thickness versus nonlocal parameter – continuous: with surface effects, dashed: without surface effects.

Fig 6 depicts the load ratio (77) for a simply supported square nanoplate versus the nonlocal parameter μ, with and without surface effects, for various slopes of thickness variation. The ratio is larger for constant thickness, lower for linear and the lowest for quadratic thickness. Besides, the difference between the results with and without surface effects decreases as the order of the thickness variation increases from constant to quadratic. It is also observed that the slope of variation with respect to the increase of the nonlocal parameter is the same for all cases.

Fig 7 depicts variation of the buckling load ratio versus nonlocal parameter μ for CCCC square nanoplate. Some dedications from the previous case with SSSS edges are concurrent here as well. The difference between consideration and not consideration of the surface effects decreases with increase of the thickness variation order, but remains rather unchanged for various values of μ. Unlike the SSSS nanoplate in which the relation between λ and μ is nearly linear, the CCCC nanoplate has steeper decrease in λ for lower values of μ.

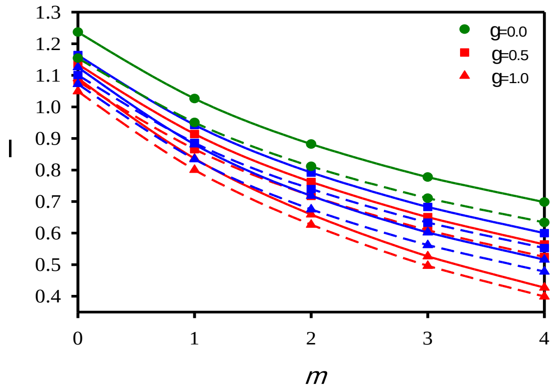

Fig 7. Biaxial buckling load ratio of CCCC square nanoplate with constant (green), linear (blue) and quadratic (red) thickness versus nonlocal parameter – continuous: with surface effects, dashed: without surface effects.

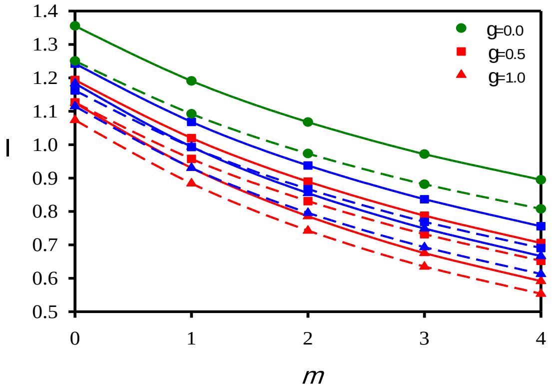

Fig 8. Biaxial buckling load ratio of CCSS square nanoplate with constant (green), linear (blue) and quadratic (red) thickness versus nonlocal parameter – continuous: with surface effects, dashed: without surface effects.

Fig 8 depicts variation of the buckling load ratio versus nonlocal parameter μ for CCSS square nanoplate. Compared to Figs 6 and 7, one may find that the behavior is nearer to CCCC boundary conditions, which indicates that the clamped edges dominate the structural behavior rather than the simple edges.

Figs 9-11 show variation of the buckling load ratio versus elastic foundation parameter K_W for CCCC, SSSS and CCSS square nanoplates. In all of them, the relationship between λ and K_W is almost linear, whose slope is steeper for lower values of n and simple edges. Again, it is seen that λ differs less with surface effects for quadratic thickness than the linear or constant thickness. Moreover, as the difference between the thickness at the left and right edges increases, the ratio decreases for all cases. Besides, the CCSS case is nearer to the CCCC case, reflecting dominance of the clamped edges over simple edges in structural behavior. It is clearly seen that there is an almost direct relationship between increase of the elastic foundation stiffness and the load ratio in all cases. Existence of surface effects has definitely increased the load ratio as well, but the increasing range is slightly more when the foundation parameter is equal to zero. For non-zero K_W, the effect of surface layer remains rather unchanged.

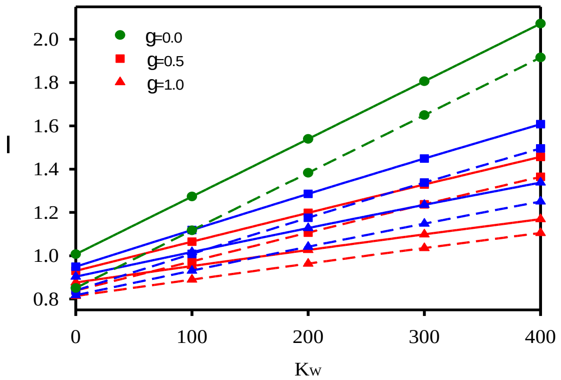

Fig 9. Biaxial buckling load ratio of SSSS square nanoplate with constant (green), linear (blue) and quadratic (red) thickness versus elastic foundation parameter K_W – continuous: with surface effects, dashed: without surface effects.

Figs 12-14 display variation of the load ratio versus the aspect ratio of the rectangular nanoplate. It is seen that the load ratio increases with increase of the aspect ratio, steeper at first but slower for higher aspect ratios, especially for clamped edges. Moreover, the difference between the cases with and without surface effects increases as the aspect ratio raises.

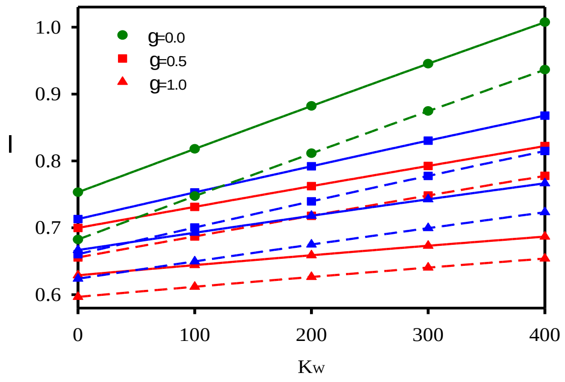

Fig 10. Biaxial buckling load ratio of CCCC square nanoplate with constant (green), linear (blue) and quadratic (red) thickness versus elastic foundation parameter K_w – continuous: with surface effects, dashed: without surface effects.

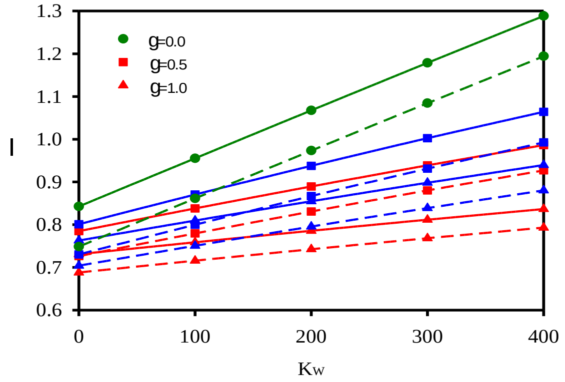

Fig 11. Biaxial buckling load ratio of CCSS square nanoplate with constant (green), linear (blue) and quadratic (red) thickness versus elastic foundation parameter K_w – continuous: with surface effects, dashed: without surface effects.

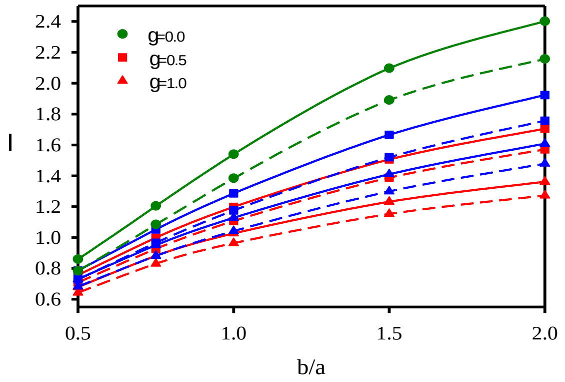

Fig 12. Biaxial buckling load ratio of SSSS nanoplate with constant (green), linear (blue) and quadratic (red) thickness versus the aspect ratio – continuous: with surface effects, dashed: without surface effects.

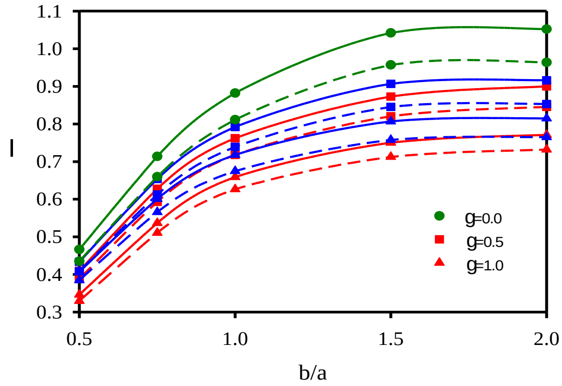

Fig 13. Biaxial buckling load ratio of CCCC nanoplate with constant (green), linear (blue) and quadratic (red) thickness versus the aspect ratio – continuous: with surface effects, dashed: without surface effects.

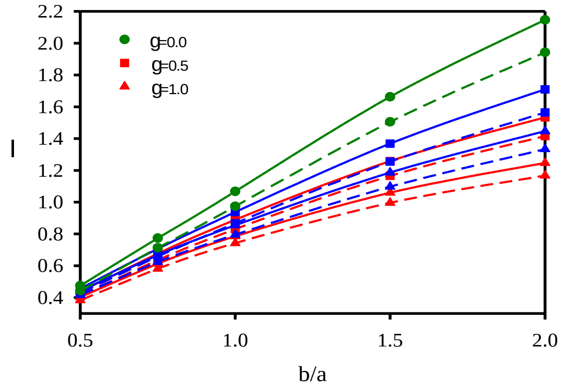

Fig 14. Biaxial buckling load ratio of CCSS nanoplate with constant (green), linear (blue) and quadratic (red) thickness versus the aspect ratio – continuous: with surface effects, dashed: without surface effects.

While nanoplates with simple and clamped edges have been vastly discussed in the literature, those having free or guided edges were much less visited. The remainder of this section will present some detailed results on the behavior of such nanoplates to make comparisons with the former cases. The same configuration and material properties as the previous models is considered here. The elastic foundation is also imported by $K_W = 200$ and $K_S = 0$. Fig 15 shows variation of the load ratio for SSFF nanoplate versus the nonlocal parameter, in various cases of thickness variation with and without surface effects. Compared with more rigid edges such as simple and clamped, higher ratios are visible here, which are only slightly affected by increase of the nonlocal parameter. A rather similar behavior is visible in Fig 16 for SSGG nanoplate, albeit the ratios are globally less than those of SSFF for constant thickness, and their difference decays with increase of the thickness variation order. This shows that the edges without shear constraints as free and guided types, are more sensitive to the effect of elastic foundations, but less sensitive to nonlocal effects. By inclusion of a more rigid edge, i.e. SSCF configuration in Fig 17, the structural behavior clearly tends to that of previous figures, i.e. overall decrease of the load ratio, and more affection by the nonlocal parameter.

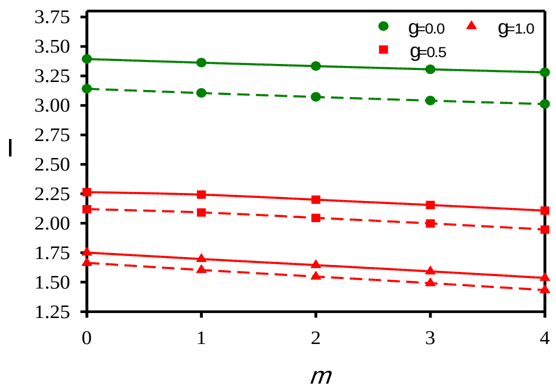

Fig 15. Biaxial buckling load ratio of SSFF nanoplate with constant (green) and linear (red) thickness versus the nonlocal parameter – continuous: with surface effects, dashed: without surface effects.

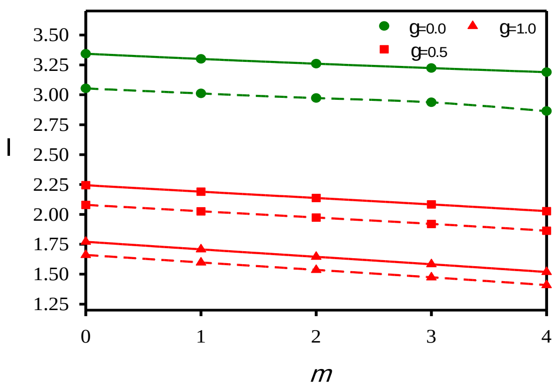

Fig 16. Biaxial buckling load ratio of SSGG nanoplate with constant (green) and linear (red) thickness versus the nonlocal parameter – continuous: with surface effects, dashed: without surface effects.

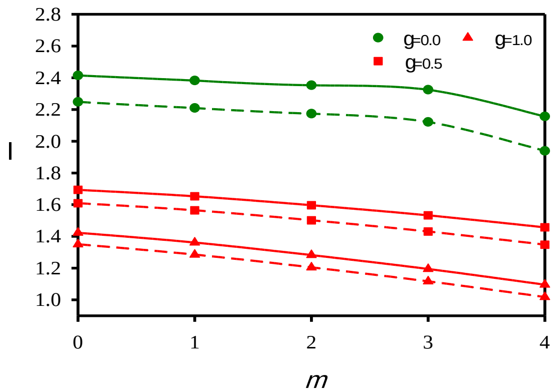

Fig 17. Biaxial buckling load ratio of SSCF nanoplate with constant (green) and linear (red) thickness versus the nonlocal parameter – continuous: with surface effects, dashed: without surface effects.

5.2. Free vibration analysis

In this section, we elaborate on the effect of various parameters, as the ones in previous section, on free vibration behavior of the nanoplates with elastic foundation, surface effects and variable thickness. The bulk and surface material properties, as well as geometric configuration, is similar to those in the previous section. The oncoming diagrams report the following fundamental frequency ratio,

$$\varpi = \frac{\text{Fundamental frequency with size effect, surface effect or elastic foundation}}{\text{Fundamental frequency without size effect, surface effect and elastic foundation}} \tag{78}$$

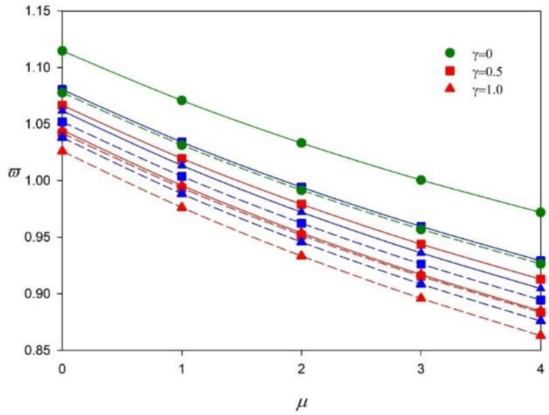

Fig 18. Fundamental frequency ratio of CCCC square nanoplate with constant (green), linear (blue) and quadratic (red) thickness versus nonlocal parameter – continuous: with surface effects, dashed: without surface effects.

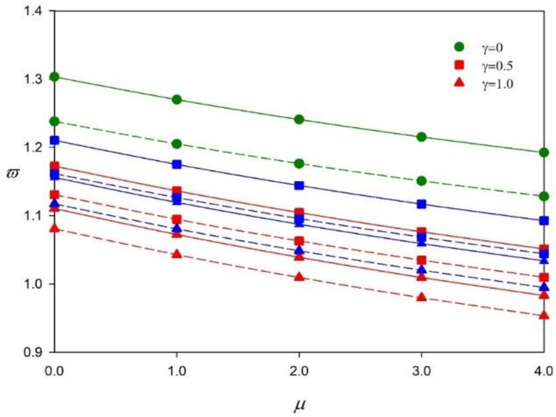

Fig 19. Fundamental frequency ratio of SSSS square nanoplate with constant (green), linear (blue) and quadratic (red) thickness versus nonlocal parameter – continuous: with surface effects, dashed: without surface effects.

Figs 18-20 depict the above frequency ratio for CCCC, SSSS and CCSS edges, respectively. By increasing the rigidity of the edges, the ratio decreases meaningfully. Besides, as the order of the thickness variation function increases from zero (constant thickness) to two (quadratic thickness variation), the ratio decreases considerably. The nonlocal parameter has an adverse effect on rigidity of the nanoplates, and reduces the ratio significantly.

Figs 21-23 show the effect of elastic foundation parameter K_W on the frequency ratio, while keeping K_S zero, for fully clamped, simply supported and mixed (CCSS) edges, respectively. As seen, by reducing the rigidity of the edges, the variation range of the ratio increases. Besides, increasing the difference between the thickness at the left and right sides of the nanoplate decreases the variation of the frequency ratio with respect to K_W. Moreover, the surface effects are more critical for the cases with constant thickness than the linear, and more for linear than the quadratic thickness variation.

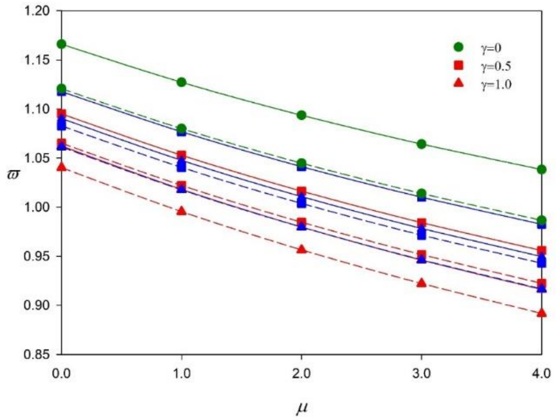

Fig 20. Fundamental frequency ratio of CCSS square nanoplate with constant (green), linear (blue) and quadratic (red) thickness versus nonlocal parameter – continuous: with surface effects, dashed: without surface effects.

It is observed in Figs 21-23 that the stiffness of the elastic foundation has an almost direct relationship with the frequency ratio. On the other hands, both increasing the foundation stiffness as well as considering surface effects increases the frequency ratio, but the variation is slightly more for smaller values of K_W . The behavior is rather similar to what happened for buckling analysis in the previous section.

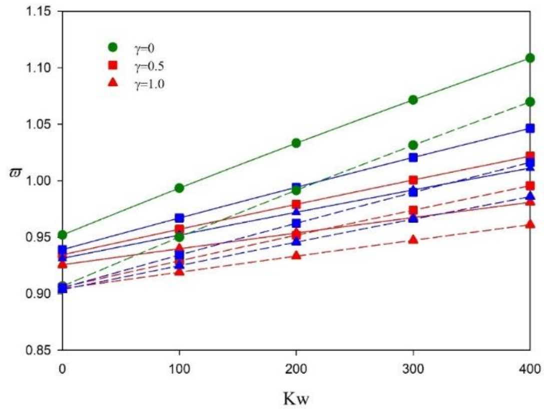

Fig 21. Fundamental frequency ratio of CCCC square nanoplate with constant (green), linear (blue) and quadratic (red) thickness versus elastic foundation parameter K_W – continuous: with surface effects, dashed: without surface effects.

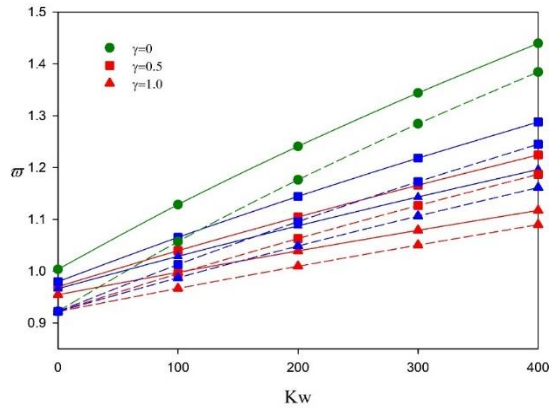

Fig 22. Fundamental frequency ratio of SSSS square nanoplate with constant (green), linear (blue) and quadratic (red) thickness versus elastic foundation parameter K_W – continuous: with surface effects, dashed: without surface effects.

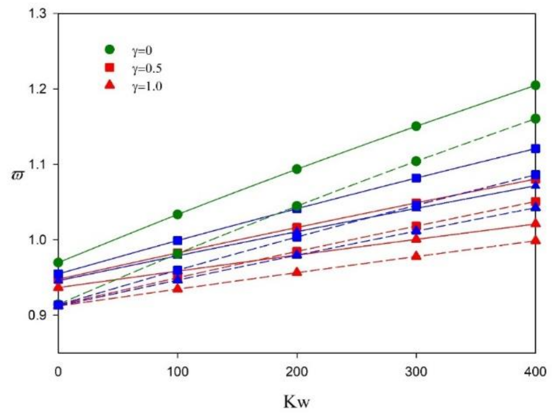

Fig 23. Fundamental frequency ratio of CCSS square nanoplate with constant (green), linear (blue) and quadratic (red) thickness versus elastic foundation parameter K_w – continuous: with surface effects, dashed: without surface effects.

Figs 24-26 show the effect of varying the aspect ratio of the nanoplate on the frequency ratio for CCCC, SSSS and CCSS boundary conditions, respectively. As seen, for less rigid edges, the variation range has widened. Moreover, the surface effect is better seen for constant thickness than the two others.

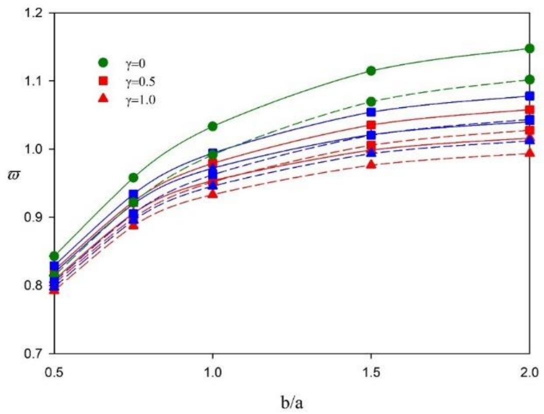

Fig 24. Fundamental frequency ratio of CCCC nanoplate with constant (green), linear (blue) and quadratic (red) thickness versus the aspect ratio – continuous: with surface effects, dashed: without surface effects.

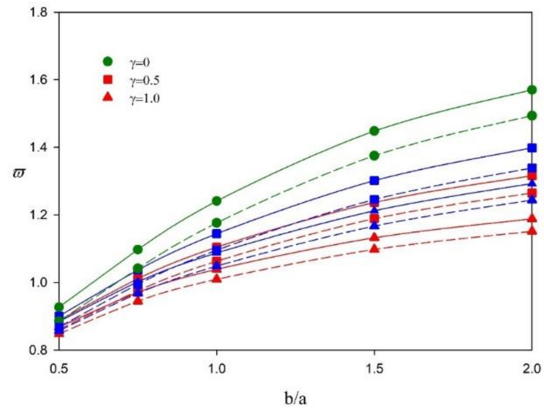

Fig 25. Fundamental frequency ratio of SSSS nanoplate with constant (green), linear (blue) and quadratic (red) thickness versus the aspect ratio – continuous: with surface effects, dashed: without surface effects.

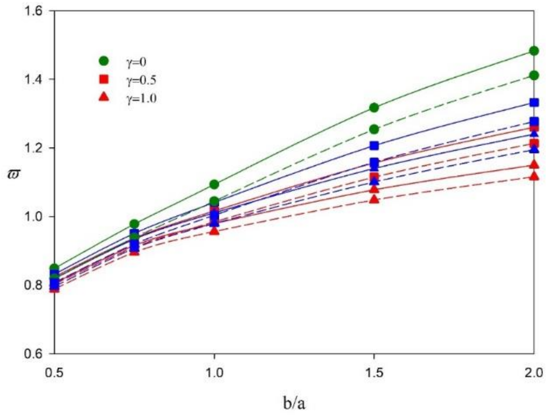

Fig 26. Fundamental frequency ratio of CCSS nanoplate with constant (green), linear (blue) and quadratic (red) thickness versus the aspect ratio – continuous: with surface effects, dashed: without surface effects.

Finally, to make a comparison with less before seen boundary conditions of free and guided, Figs 27-29 present the nonlocal effect on the frequency ratio for SSFF, SSGG and SSCF nanoplates, respectively. The nonlocal effect on these cases is only slightly felt in the mentioned figures, with a linear correlation. Besides, the SSFF and SSGG nanoplates are much closer to each other than they used to be for buckling tests. Again, the nanoplate with constant thickness has the highest ratio then is the linear and the least ratio is for quadratic thickness. Introduction of clamped edge in Fig. 29 has decreased the overall ratios, but still shows the linear correlation between ϖ and μ .

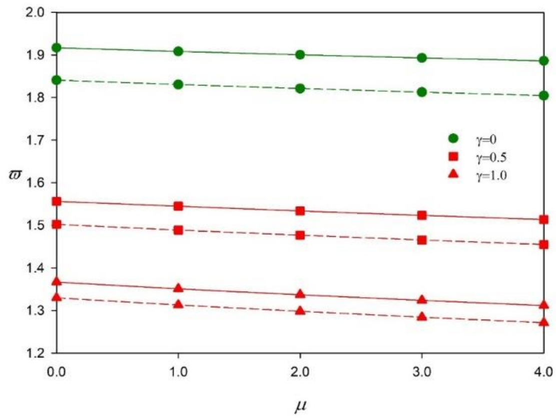

Fig 27. Fundamental frequency ratio of SSFF nanoplate with constant (green) and linear (red) thickness versus the nonlocal parameter – continuous: with surface effects, dashed: without surface effects.

As an overall conclusion, heterogeneity due to variable thickness, causes some parts of the nanoplate be less flexible than some other parts of it, unlike homogeneous nanoplates that have the same rigidity all over the domain. The difference in rigidity at various parts of the domain causes the waves by the mode shapes in buckling or free vibration to form in more flexible areas. This increases the effect of the edge support nearer to the flexible parts in the overall behavior. For free vibration problems in nanoplates with variable thickness, since the distribution of the mass per area and the rigidity follows rather similar rules, the frequency characteristics will tend to those of a homogeneous nanoplate with its constant thickness equal to the average of the variable thickness. For buckling problems, on the other hand, since the in-plane load is the same all over the area, a local instability may occur in more flexible parts of the nanoplate and thus, the critical load is lower than that of the homogeneous nanoplate having its average thickness. As also seen in the given results, the value of the nonlocal parameter does not change the intensity of thickness variation effectiveness, with and without surface effects, but the overall ratio is altered similarly throughout the range.

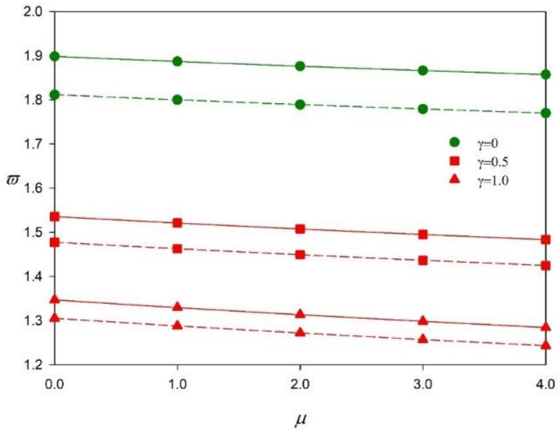

Fig 28. Fundamental frequency ratio of SSGG nanoplate with constant (green) and linear (red) thickness versus the nonlocal parameter – continuous: with surface effects, dashed: without surface effects.

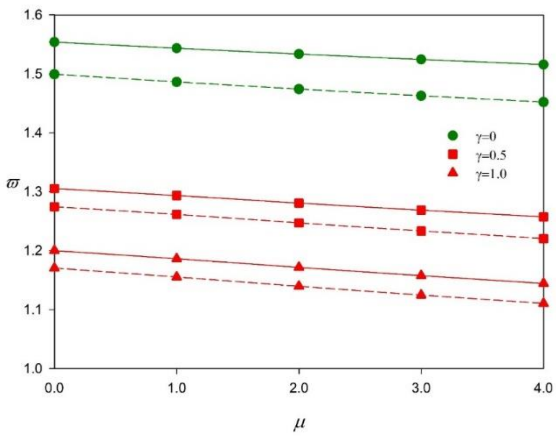

Fig 29. Fundamental frequency ratio of SSCF nanoplate with constant (green) and linear (red) thickness versus the nonlocal parameter – continuous: with surface effects, dashed: without surface effects.

6. Conclusions

We developed a simple and versatile framework for buckling and free vibration analysis of rectangular nanoplates based on nonlocal theory, with the possibility of in-plane variable properties, elastic foundation and surface effects. The solution method was formulated based on equilibrated basis functions. The PDE is approximately satisfied through a weighted residual approach, while the boundary conditions are strongly applied in a collocation style. The use of global basis functions brings complete continuity to the displacement function over the nanoplate surface. The 2D integrals are evaluated by linear combination of pre-evaluated single integrals, therefore removing the numerical quadrature step. Verification of the proposed formulation showed quite accurate and effective for various problems. While the method has shown very good accuracy and convergence for rectangular nano plates, its applicability to concave domains or internally perforated plates may have difficulties due to the so called pollution error, which will be widespread in global domain methods such as the one here. This may be resolved by a localized formulation of the method, such as the one in [70].

The method was then used to analyse the buckling and free vibration of sample nanoplates with variable thickness, leading to in-plane variable mass-per-area and stiffness, for various combinations of boundary conditions. For unification, the buckling load ratio or fundamental frequency ratio with respect to the completely classic configuration was reported. It was deduced that the effect of nonlocal parameter on the ratio decreases by the increase of the variation order of the thickness from constant to quadratic. Also, the surface effects are more affecting for constant than linear, and for linear than the quadratic thickness variation. Investigation of various boundary conditions showed that free or guided edges result higher ratios than clamped or simple edges, and their diagrams versus the nonlocal parameter tend to linear style, with slight change of the load/frequency ratio versus nonlocal parameter. Meanwhile, the effect of free edges in the overall behavior of the diagrams showed dominant over simple or clamped edges, and the clamped edge showed also dominant over simple edge, in terms of affecting the behavior of the related diagrams. The new results may also be of interest for the researchers on similar fields.

References

[1] S. Rathinavel, K. Priyadharshini, D. Panda, A review on carbon nanotube: An overview of synthesis, properties, functionalization, characterization, and the application, *Materials Science and Engineering: B,* Vol. 268, pp. 115095, 2021.

[2] X. Sun, P. Cheng, H. Wang, H. Xu, L. Dang, Z. Liu, Z. Lei, Activation of graphene aerogel with phosphoric acid for enhanced electrocapacitive performance, *Carbon,* Vol. 92, pp. 1-10, 2015.

[3] J.-Z. Liang, Q. Du, G. C.-P. Tsui, C.-Y. Tang, Tensile properties of graphene nano-platelets reinforced polypropylene composites, *Composites Part B: Engineering,* Vol. 95, pp. 166-171, 2016.

[4] N. I. Goktas, P. Wilson, A. Ghukasyan, D. Wagner, S. McNamee, R. LaPierre, Nanowires for energy: A review, *Applied Physics Reviews,* Vol. 5, No. 4, 2018.

[5] S. Narendar, S. Gopalakrishnan, A nonlocal continuum mechanics model to estimate the material property of single-walled carbon nanotubes, *International Journal of Nanoscience,* Vol. 11, No. 01, pp. 1250007, 2012.

[6] M. Shaat, A. Abdelkefi, New insights on the applicability of Eringen's nonlocal theory, *International Journal of Mechanical Sciences,* Vol. 121, pp. 67-75, 2017.

[7] E. Tomboulis, Nonlocal and quasilocal field theories, *Physical Review D,* Vol. 92, No. 12, pp. 125037, 2015.

[8] A. R. Hadjesfandiari, G. F. Dargush, Couple stress theory for solids, *International Journal of Solids and Structures*, Vol. 48, No. 18, pp. 2496-2510, 2011.

[9] A. Shakouri, T. Ng, R. Lin, A study of the scale effects on the flexural vibration of graphene sheets using REBO potential based atomistic structural and nonlocal couple stress thin plate models, *Physica E: Low-dimensional Systems and Nanostructures,* Vol. 50, pp. 22-28, 2013.

[10] H. Salehipour, A. Shahidi, H. Nahvi, Modified nonlocal elasticity theory for functionally graded materials, *International Journal of Engineering Science,* Vol. 90, pp. 44-57, 2015.

[11] Z. Mousavi, S. A. Shahidi, B. Boroomand, A new method for bending and buckling analysis of rectangular nano plate: full modified nonlocal theory, *Meccanica,* Vol. 52, pp. 2751-2768, 2017.

[12] X. Xu, D. Rong, C. Lim, C. Yang, Z. Zhou, An analytical symplectic approach to the vibration analysis of orthotropic graphene sheets, *Acta Mechanica Sinica,* Vol. 33, pp. 912-925, 2017.

[13] N. M. Ali, N. H. Rafat, Modeling and simulation of nanorods photovoltaic solar cells: A review, *Renewable and Sustainable Energy Reviews,* Vol. 68, pp. 212-220, 2017.

[14] M. Ö. Yayli, Axial vibration analysis of a Rayleigh nanorod with deformable boundaries, *Microsystem Technologies,* Vol. 26, pp. 2661-2671, 2020.

[15] A. Celis, M. N. Nair, A. Taleb-Ibrahimi, E. H. Conrad, C. Berger, W. De Heer, A. Tejeda, Graphene nanoribbons: fabrication, properties and devices, *Journal of Physics D: Applied Physics,* Vol. 49, No. 14, pp. 143001, 2016.

[16] F. P. Pinnola, M. S. Vaccaro, R. Barretta, F. M. de Sciarra, Finite element method for stress-driven nonlocal beams, *Engineering Analysis with Boundary Elements,* Vol. 134, pp. 22-34, 2022.

[17] M. Ö. Yayli, Buckling analysis of a microbeam embedded in an elastic medium with deformable boundary conditions, *Micro & Nano Letters,* Vol. 11, No. 11, pp. 741-745, 2016.

[18] H. M. Numanoğlu, H. Ersoy, B. Akgöz, Ö. Civalek, A new eigenvalue problem solver for thermo-mechanical vibration of Timoshenko nanobeams by an innovative nonlocal finite element method, *Mathematical Methods in the Applied Sciences,* Vol. 45, No. 5, pp. 2592-2614, 2022.

[19] X. Xu, B. Karami, M. Janghorban, On the dynamics of nanoshells, *International Journal of Engineering Science,* Vol. 158, pp. 103431, 2021.

[20] M. Bastami, B. Behjat, Free vibration and buckling investigation of piezoelectric nano-plate in elastic medium considering nonlocal effects, *Journal of the Brazilian Society of Mechanical Sciences and Engineering,* Vol. 40, pp. 1-7, 2018.

[21] S. Pradhan, T. Murmu, Small scale effect on the buckling analysis of single-layered graphene sheet embedded in an elastic medium based on nonlocal plate theory, *Physica E: Low-dimensional Systems and Nanostructures*, Vol. 42, No. 5, pp. 1293-1301, 2010.

[22] S. M. Monavari, F. Marsusi, N. Memarian, M. Qasemnazhand, Carbon nanotubes and nanobelts as potential materials for biosensor, *Scientific reports,* Vol. 13, No. 1, pp. 3118, 2023.

[23] Ö. Civalek, M. Avcar, Free vibration and buckling analyses of CNT reinforced laminated non-rectangular plates by discrete singular convolution method, *Engineering with Computers,* Vol. 38, No. Suppl 1, pp. 489-521, 2022.
[24] J. Reddy, Nonlocal nonlinear formulations for bending of classical and shear deformation theories of beams and plates, *International Journal of Engineering Science*, Vol. 48, No. 11, pp. 1507-1518, 2010.
[25] T. Aksencer, M. Aydogdu, Levy type solution method for vibration and buckling of nanoplates using nonlocal elasticity theory, *Physica E: Low-dimensional Systems and Nanostructures,* Vol. 43, No. 4, pp. 954-959, 2011.
[26] R. Ansari, S. Sahmani, Prediction of biaxial buckling behavior of single-layered graphene sheets based on nonlocal plate models and molecular dynamics simulations, *Applied Mathematical Modelling,* Vol. 37, No. 12-13, pp. 7338-7351, 2013.
[27] T. Murmu, J. Sienz, S. Adhikari, C. Arnold, Nonlocal buckling of double-nanoplate-systems under biaxial compression, *Composites Part B: Engineering,* Vol. 44, No. 1, pp. 84-94, 2013.
[28] Y. Li, Z. Cai, S. Shi, Buckling and free vibration of magnetoelectroelastic nanoplate based on nonlocal theory, *Composite Structures*, Vol. 111, pp. 522-529, 2014.
[29] H.-S. Shen, L. Shen, C.-L. Zhang, Nonlocal plate model for nonlinear bending of single-layer graphene sheets subjected to transverse loads in thermal environments, *Applied Physics A,* Vol. 103, pp. 103-112, 2011.
[30] H. Babaei, A. Shahidi, Free vibration analysis of quadrilateral nanoplates based on nonlocal continuum models using the Galerkin method: the effects of small scale, *Meccanica,* Vol. 48, pp. 971-982, 2013.
[31] E. Ruocco, J. Reddy, Buckling analysis of elastic–plastic nanoplates resting on a Winkler–Pasternak foundation based on nonlocal third-order plate theory, *International Journal of Non-Linear Mechanics,* Vol. 121, pp. 103453, 2020.
[32] M. Karamooz Ravari, S. Talebi, A. Shahidi, Analysis of the buckling of rectangular nanoplates by use of finite-difference method, *Meccanica,* Vol. 49, pp. 1443-1455, 2014.
[33] M. Al-Furjan, L. Shan, X. Shen, R. Kolahchi, D. K. Rajak, Combination of FEM-DQM for nonlinear mechanics of porous GPL-reinforced sandwich nanoplates based on various theories, *Thin-Walled Structures,* Vol. 178, pp. 109495, 2022.
[34] H. Fazeli, A. Adamian, A. Hosseini-Sianaki, Influence of initial geometric imperfection on static and free vibration analyses of porous FG nanoplate using an isogeometric approach, *Journal of the Brazilian Society of Mechanical Sciences and Engineering,* Vol. 43, No. 4, pp. 200, 2021.
[35] P.-C. Nguyen, Q.-H. Pham, A nonlocal isogeometric model for buckling and dynamic instability analyses of FG graphene platelets-reinforced nanoplates, *Materials Today Communications,* Vol. 34, pp. 105211, 2023.
[36] M. Ghadiri, N. Shafiei, H. Alavi, Thermo-mechanical vibration of orthotropic cantilever and propped cantilever nanoplate using generalized differential quadrature method, *Mechanics of Advanced Materials and Structures,* Vol. 24, No. 8, pp. 636-646, 2017.
[37] N. Noormohammadi, A. M. Asadi, P. Mohammadi Dashtaki, B. Boroomand, Buckling and free vibration analysis of in-plane heterogeneous nanoplates using a simple boundary method, *Journal of the Brazilian Society of Mechanical Sciences and Engineering,* Vol. 45, No. 5, pp. 267, 2023.
[38] P. Mohammadi Dashtaki, N. Noormohammadi, Static analysis of orthotropic nanoplates reinforced by defective graphene based on strain gradient theory using a simple boundary method, *Acta Mechanica,* Vol. 234, No. 11, pp. 5203-5228, 2023.
[39] J. Liu, R. Wu, R. Xia, Surface effects at the nanoscale based on Gurtin's theory: a review, *Journal of the Mechanical Behavior of Materials,* Vol. 23, No. 5-6, pp. 141-151, 2014.
[40] R. Ansari, S. Sahmani, Surface stress effects on the free vibration behavior of nanoplates, *International Journal of Engineering Science*, Vol. 49, No. 11, pp. 1204-1215, 2011.
[41] A. Assadi, Size dependent forced vibration of nanoplates with consideration of surface effects, *Applied Mathematical Modelling,* Vol. 37, No. 5, pp. 3575-3588, 2013.
[42] M. Mohammadimehr, M. Mohammadimehr, P. Dashti, Size-dependent effect on biaxial and shear nonlinear buckling analysis of nonlocal isotropic and orthotropic micro-plate based on surface stress and modified couple stress theories using differential quadrature method, *Applied Mathematics and Mechanics,* Vol. 37, pp. 529-554, 2016.
[43] M. Karimi, H. R. Mirdamadi, A. R. Shahidi, Positive and negative surface effects on the buckling and vibration of rectangular nanoplates under biaxial and shear in-plane loadings based on nonlocal elasticity theory, *Journal of the Brazilian Society of Mechanical Sciences and Engineering,* Vol. 39, pp. 1391-1404, 2017.

[44] F. Kamali, F. Shahabian, Analytical solutions for surface stress effects on buckling and post-buckling behavior of thin symmetric porous nano-plates resting on elastic foundation, *Archive of applied mechanics,* Vol. 91, pp. 2853-2880, 2021.

[45] K. M. Liew, X. He, S. Kitipornchai, Predicting nanovibration of multi-layered graphene sheets embedded in an elastic matrix, *Acta materialia,* Vol. 54, No. 16, pp. 4229-4236, 2006.

[46] S. Pradhan, A. Kumar, Vibration analysis of orthotropic graphene sheets embedded in Pasternak elastic medium using nonlocal elasticity theory and differential quadrature method, *Computational Materials Science,* Vol. 50, No. 1, pp. 239-245, 2010.

[47] A. Assadi, B. Farshi, Size dependent stability analysis of circular ultrathin films in elastic medium with consideration of surface energies, *Physica E: Low-dimensional Systems and Nanostructures,* Vol. 43, No. 5, pp. 1111-1117, 2011.

[48] L. Tong, B. Wen, Y. Xiang, Z. Lei, C. Lim, Elastic buckling of nanoplates based on general third-order shear deformable plate theory including both size effects and surface effects, *International Journal of Mechanics and Materials in Design,* Vol. 17, No. 3, pp. 521-543, 2021.

[49] M. Mohammadimehr, M. M. Mohammadi Najafabadi, H. Nasiri, B. Rousta Navi, Surface stress effects on the free vibration and bending analysis of the nonlocal single-layer graphene sheet embedded in an elastic medium using energy method, *Proceedings of the Institution of Mechanical Engineers, Part N: Journal of Nanomaterials, Nanoengineering and Nanosystems,* Vol. 230, No. 3, pp. 148-160, 2016.

[50] N. Radić, D. Jeremić, S. Trifković, M. Milutinović, Buckling analysis of double-orthotropic nanoplates embedded in Pasternak elastic medium using nonlocal elasticity theory, *Composites Part B: Engineering,* Vol. 61, pp. 162-171, 2014.

[51] T. Banh-Thien, H. Dang-Trung, L. Le-Anh, V. Ho-Huu, T. Nguyen-Thoi, Buckling analysis of non-uniform thickness nanoplates in an elastic medium using the isogeometric analysis, *Composite Structures,* Vol. 162, pp. 182-193, 2017.

[52] A. R. Motamedi, B. Boroomand, N. Noormohammadi, A Trefftz based meshfree local method for bending analysis of arbitrarily shaped laminated composite and isotropic plates, *Engineering Analysis with Boundary Elements,* Vol. 143, pp. 237-262, 2022.

[53] A. R. Motamedi, N. Noormohammadi, B. Boroomand, A novel Trefftz-based meshfree method for free vibration and buckling analysis of thin arbitrarily shaped laminated composite and isotropic plates, *Computers & Mathematics with Applications,* Vol. 145, pp. 318-340, 2023.

[54] Y. Hon, T. Wei, A fundamental solution method for inverse heat conduction problem, *Engineering analysis with boundary elements,* Vol. 28, No. 5, pp. 489-495, 2004.

[55] B. Shamsaei, B. Boroomand, Exponential basis functions in solution of laminated structures, *Composite Structures,* Vol. 93, No. 8, pp. 2010-2019, 2011.

[56] A. R. Motamedi, N. Noormohammadi, B. Boroomand, A novel highly accurate Trefftz attitude towards bending and free vibration analysis of doubly-curved laminated and sandwich shallow shells, *Engineering Analysis with Boundary Elements,* Vol. 162, pp. 337-361, 2024.

[57] N. Noormohammadi, B. Boroomand, A boundary method using equilibrated basis functions for bending analysis of in-plane heterogeneous thick plates, *Archive of Applied Mechanics,* Vol. 91, pp. 487-507, 2021.

[58] M. Azizpooryan, N. Noormohammadi, B. Boroomand, Equilibrated basis functions for static analysis of in-plane heterogeneous laminated composite plates in boundary and meshfree approaches, *Iranian Journal of Science and Technology, Transactions of Mechanical Engineering*, pp. 1-28, 2022.

[59] O. Bateniparvar, N. Noormohammadi, An enrichment technique for bending analysis of in-plane heterogeneous thin plates with weak singularities, *Engineering with Computers,* Vol. 39, No. 5, pp. 3131-3153, 2023.

[60] A. Farajpour, M. Danesh, M. Mohammadi, Buckling analysis of variable thickness nanoplates using nonlocal continuum mechanics, *Physica E: Low-dimensional Systems and Nanostructures,* Vol. 44, No. 3, pp. 719-727, 2011.

[61] M. R. Barati, A. M. Zenkour, Analysis of postbuckling behavior of general higher-order functionally graded nanoplates with geometrical imperfection considering porosity distributions, *Mechanics of Advanced Materials and Structures,* Vol. 26, No. 12, pp. 1081-1088, 2019.

[62] J. N. Reddy, 2003, *Mechanics of laminated composite plates and shells: theory and analysis*, CRC press,

[63] T. J. Rivlin, 2020, *Chebyshev polynomials*, Courier Dover Publications,

[64] N. Noormohammadi, B. Boroomand, A fictitious domain method using equilibrated basis functions for harmonic and bi-harmonic problems in physics, *Journal of Computational Physics,* Vol. 272, pp. 189-217, 2014.

[65] K. Behfar, R. Naghdabadi, Nanoscale vibrational analysis of a multi-layered graphene sheet embedded in an elastic medium, *Composites science and technology,* Vol. 65, No. 7-8, pp. 1159-1164, 2005.

[66] M. H. Omurtag, A. Özütok, A. Y. Aköz, Y. OeZCELİKOeRS, Free vibration analysis of Kirchhoff plates resting on elastic foundation by mixed finite element formulation based on Gateaux differential, *International journal for numerical methods in engineering,* Vol. 40, No. 2, pp. 295-317, 1997.

[67] A. M. Zenkour, Vibration analysis of a single-layered graphene sheet embedded in visco-Pasternak's medium using nonlocal elasticity theory, *Journal of Vibroengineering*, Vol. 18, No. 4, pp. 2319-2330, 2016.

[68] X. Zheng, M. Huang, D. An, C. Zhou, R. Li, New analytic bending, buckling, and free vibration solutions of rectangular nanoplates by the symplectic superposition method, *Scientific Reports,* Vol. 11, No. 1, pp. 2939, 2021.

[69] B. Singh, V. Saxena, Transverse vibration of a rectangular plate with bidirectional thickness variation, *Journal of Sound and Vibration*, Vol. 198, No. 1, pp. 51-65, 1996.

[70] N. Noormohammadi, D. Afifi, B. Boroomand, O. Bateniparvar, A meshfree method for the solution of 2D and 3D second order elliptic boundary value problems in heterogeneous media, *Mathematics and Computers in Simulation,* Vol. 213, pp. 274-301, 2023.